IFIT1 is rapidly evolving and exhibits disparate antiviral activities across 11 mammalian orders

Matthew B. McDougal[1], Ian N. Boys[1], Anthony M. De Maria[1], Emi Nakahara[1], and John W. Schoggins[1]*

[1]Department of Microbiology, University of Texas Southwestern Medical Center, Dallas, TX, USA

*To whom correspondence may be addressed. **Email:** john.schoggins@utsouthwestern.edu

Abstract

Mammalian mRNAs possess an N7-methylguanosine (m7G) cap and 2'O methylation of the initiating nucleotide at their 5' end, whereas certain viral RNAs lack these characteristic features. The human antiviral restriction factor IFIT1 recognizes and binds to specific viral RNAs that lack the 5' features of host mRNAs, resulting in targeted suppression of viral RNA translation. This interaction imposes significant host-driven evolutionary pressures on viruses, and many viruses have evolved mechanisms to evade the antiviral action of human IFIT1. However, little is known about the virus-driven pressures that may have shaped the antiviral activity of IFIT1 genes across mammals. Here, we take an evolution-guided approach to show that the IFIT1 gene is rapidly evolving in multiple mammalian clades, with positive selection acting upon several residues in distinct regions of the protein. In functional assays with 39 IFIT1s spanning diverse mammals, we demonstrate that IFIT1 exhibits a range of antiviral phenotypes, with many orthologs lacking antiviral activity against viruses that are strongly suppressed by other IFIT1s. We further show that IFIT1s from human and a bat, the black flying fox, inhibit Venezuelan equine encephalitis virus (VEEV) and strongly bind to Cap0 RNAs. Unexpectedly, chimpanzee IFIT1, which differs from human IFIT1 by only 8 amino acids, does not inhibit VEEV infection and exhibits minimal Cap0 RNA-binding. In mutagenesis studies, we determine that amino acids 364 and 366, the latter of which is rapidly evolving, are sufficient to confer the differential anti-VEEV activity between human and chimpanzee IFIT1. These data suggest that virus-host genetic conflicts have influenced the antiviral specificity of IFIT1 across diverse mammalian orders.

Introduction

Interferon-induced protein with tetratricopeptide repeats 1 (IFIT1) is an interferon-stimulated gene (ISG) effector that distinguishes self and non-self RNA. Mammalian mRNAs possess an N7-methylguanosine (m7G) cap and 2′O methylation of the initiating nucleotide, whereas many viral RNAs lack one or both features. IFIT1 binds uncapped 5′-triphosphate RNA (5′-ppp-RNA) and capped but unmethylated RNA (Cap0, an m^7G cap lacking 2′-O methylation) (1-3). IFIT1 binding to viral RNA inhibits infection by decreasing the amount of accessible RNA from the pool of replicating viral RNA (4) and by interacting with eIF proteins required for translation of viral proteins (5).

This restriction imposes a host-driven evolutionary pressure for viruses to evade IFIT1 through various mechanisms (5). Some encode their own capping and 2’O methyltransferase enzymes, translate through internal ribosome entry sites (IRES), hijack host mRNA caps by cap-snatching, or mask the 5' end with RNA structures (5). For the alphavirus Venezuelan equine encephalitis virus (VEEV), which has a positive-sense, single-stranded RNA genome, a 5’ UTR structure in the pathogenic Trinidad strain occludes IFIT1 binding, whereas a single-nucleotide change in the attenuated TC-83 strain destabilizes the structure and allows inhibition (1). VEEV TC-83 is sensitive to human IFIT1 and mouse Ifit1B, indicating at least partial conservation of antiviral function by IFIT proteins. Viral countermeasures may therefore drive adaptive changes in IFIT1, yet the scope of this pressure across mammalian IFIT1 remains unclear.

Pathogenic viruses can cause severe disease or death in mammals, imposing a major selective pressure on the host to evolve antiviral defenses. Viruses face reciprocal pressure to evade these defenses. These 'molecular arms races' leave signatures of positive selection in many immune genes. Positive selection, or rapid evolution, is denoted by a high ratio of nonsynonymous to synonymous substitutions (dN/dS > 1). Computational evolutionary analyses

100 of antiviral ISGs have revealed specific domains and residues that are rapidly evolving (6-8).
101 Several methods can determine if a gene, or part of a gene, is undergoing positive selection.
102 These include Phylogenetic Analysis using Maximum Likelihood (PAML), Fast
103 Unconstrained Bayesian AppRoximation (FUBAR), and Mixed Effects Model of Evolution
104 (MEME). Each one is a codon-substitution model that identifies sites within a gene that evolving
105 under selection. For example, PAML tests whether a neutral-or-purifying model (M7) fits the
106 data significantly worse than one that includes positive selection (M8). Such approaches have
107 pinpointed certain domains and amino acids that determine antiviral function in effectors such
108 as MX1 and TRIM5α (9, 10). In addition to evolutionary pressure from host-pathogen molecular
109 arms races, IFIT1 evolution has also been influenced by gene loss, gene duplication, and
110 recombination with IFIT1B (11). However, the antiviral consequences of these such events have
111 only been tested functionally in a few species, and the breadth of IFIT1 diversity across
112 Mammalia remains unknown (11). Recently, in a screen for antiviral ISGs from bats, we found
113 that IFIT1 from the black flying fox displays particularly strong suppression of VEEV (12). From
114 these prior studies, we hypothesized that evolutionary pressures may have shaped "species-
115 specific" antiviral activity among IFIT1 orthologs. Accordingly, we sought to use evolutionary and
116 functional methods to interrogate differences in antiviral activity and biochemical properties of
117 mammalian IFIT1.

118 **Results**

119 *IFIT1 is rapidly evolving in major clades of mammals*

120 Many antiviral effectors exhibit signatures of positive selection (6, 7), prompting us to
121 test whether IFIT1 is similarly evolving across several diverse clades of mammals. Using PAML
122 (13), we determined that IFIT1 exhibits signatures of rapid evolution in primates, bats,
123 carnivores, and ungulates, with the weakest signal in carnivores (Fig 1A). Rodents were

124 excluded because many species lack an IFIT1 ortholog (11). While all lineages shown signs of
125 rapid evolution, carnivore IFIT1s exhibited the least significant likelihood of pervasive positive
126 selection (Fig 1A). Furthermore, each lineage contained at least two codons under selection
127 (Fig 1A). To uncover other rapidly evolving sites, we applied two codon-based models that
128 complement PAML. FUBAR uses a Bayesian framework that assumes selection as pervasive
129 across all branches of the phylogenetic tree (14); it detected at least one positively selected
130 codon in every lineage except carnivores. MEME identifies codons that experience episodic
131 selection on a subset of branches (15); it identified several such sites in each lineage we tested
132 (Fig 1C). These data indicate that positive selection has acted on multiple regions of IFIT1
133 across Mammalia.

134 Recombination between paralogous genes can affect analyses of positive selection (16),
135 and the evolution of some IFIT1 sequences has been influenced by recombination with IFIT1B
136 (11). To confirm that the sequences examined were likely IFIT1 orthologs, we aligned all IFIT1
137 sequences from this study with representative IFIT1B and IFIT3 sequences from several
138 mammals and built a maximum-likelihood tree from their C-terminal regions, as previously
139 described(11). All IFIT1 clustered together, separate from IFIT1B and IFIT3 sequences (Supp
140 Fig 1A), supporting their classification as orthologs. We further evaluated IFIT1 sequences for
141 recombination breakpoints using GARD, a genetic-algorithm approach for recombination
142 detection (16). A single breakpoint was detected in primates (codon 38) and ungulates (codon
143 188), whereas two were identified in bats (codons 33, 381) and carnivores (codons 14, 370)
144 (Supp Fig 1B).

145 The presence of GARD breakpoints prompted reanalysis of IFIT1 using only coding
146 regions located after the breakpoint in primates and ungulates or between breakpoints in bats
147 and carnivores. PAML still detected positive selection in every clade except carnivores (Supp

148 Fig 1C), which had the lowest signal of positive selection in our original analysis. Further, nearly
149 all codons flagged in the initial analysis (Fig 1A–C) were recovered when we re-ran FUBAR
150 (Supp Fig 1D) and MEME (Supp Fig 1E) on alignments trimmed after or between the GARD
151 breakpoints. Considering that sequences were trimmed, which removed certain sites previously
152 identified as rapidly evolving, almost all other possible positively selected sites were validated in
153 primates (11/12), bats (14/16), ungulates (30/37), and carnivores (2/4) across PAML, FUBAR,
154 and MEME analyses (Supp Fig 1C-E). To further clarify whether recombination could have
155 impacted these analyses, we used Recombination Detection Program 4 (RDP4) (17) to remove
156 inferred recombinant sequences from the primate alignment. Subsequent PAML, FUBAR, and
157 MEME analyses recovered 10 of the original 14 selected sites (Supp Fig 1F). Importantly,
158 codons 170, 193, and 366 in primates continued to exhibit evidence of rapid evolution in two
159 independent methods in both the GARD breakpoint-trimmed and RDP4-filtered datasets (Supp
160 Fig 1C–F). In bats, codon 193 likewise showed positive selection in two analyses of the
161 between-breakpoint alignment (Supp Fig 1C–E). While signatures of selection differed slightly
162 between the original, the post- or between-breakpoint trimmed, and RDP4-filtered datasets,
163 overall trends and in many cases residue-specific signals were consistent, highlighting the
164 robustness of the evolutionary signatures.

165 Overall, these analyses indicate that IFIT1 is rapidly evolving across multiple Mammalian
166 clades. Such widespread rapid evolution may result in functional consequences on antiviral
167 activity for an individual species or more broadly across clades of mammals. To address the first
168 prediction, we next tested for functional implications of within-species rapid evolution of IFIT1
169 using human IFIT1 as a model.

170

171

172 *Human IFIT1 residue 193 exhibits mutational resiliency*

173 We focused on three codons in primate IFIT1 – encoding V170, L193, and L366 in the
174 human ortholog – that were rapidly evolving in at least two models (Fig 1D). None of these
175 residues have been associated with RNA-binding or antiviral function (2, 3). In the crystal
176 structure of human IFIT1 bound to RNA, V170 and L366 lie outside the RNA-binding tunnel,
177 whereas L193 resides in the TPR4 loop. This loop sits between α-helices 9 and 10, forms a lid
178 over the 3′ exit of the tunnel, and helps link subdomain II to subdomain III (Fig 2A–C) (3). L193
179 in the TPR4 loop protrudes into the tunnel exit, comes into close contact with RNA (Fig 2C), and
180 is adjacent to R187, a residue essential for RNA binding and antiviral function (2). To test the
181 functional importance of L193, we knocked out endogenous IFIT1 in Huh7.5 cells with CRISPR–
182 Cas9 editing and re-expressed CRISPR-resistant IFIT1 variants carrying every possible amino-
183 acid substitution at position 193. Cells were then infected with VEEV (TC-83 strain) encoding a
184 GFP reporter (VEEV-GFP), and infection was quantified by flow cytometry (Fig 2D). Western
185 blotting determined that all IFIT1 point mutants were expressed to comparable levels (Fig 2D,
186 Bottom). All hydrophobic and positively charged mutants at position 193 inhibited VEEV similarly
187 to the wild-type (193L) IFIT1 (Fig 2D). Polar amino acids introduced at position 193 also
188 retained antiviral function (Fig 2D). Severe loss of function in anti-VEEV activity of IFIT1 was
189 only notable with glycine or proline (~50% loss of antiviral function) or with negatively charged
190 residues (~75-100% loss of antiviral function) (Fig 2D). Thus, codon 193 displays notable
191 functional resiliency, as most substitutions preserve antiviral activity. This result connects our
192 computational analysis to a concrete functional outcome within one species. We next asked
193 whether positive selection also influences interspecies differences in IFIT1 antiviral activity
194 across diverse mammalian orthologs.

195 *IFIT1 orthologs from diverse mammals demonstrate species-specific antiviral activity*

196 We next cloned 39 IFIT1 orthologs—derived from 38 mammalian species, including two
197 predicted equine sequences—into lentiviral expression vectors. These proteins share 60–98%
198 identity with human IFIT1 and span 11 orders within the superorders Euarchontoglires,
199 Laurasiatheria, Afrotheria, and Xenarthra (Fig 3A–B; Supp Table 1). All primate, bat, and
200 ungulate orthologs in this screen were also part of the PAML, FUBAR, and MEME analyses,
201 allowing us to correlate functional differences in antiviral activity with molecular evolutionary
202 analysis. Each construct carried an N-terminal HA tag for western-blot detection. Huh7.5 cells
203 transduced with these vectors were challenged with GFP-expressing VEEV or vesicular
204 stomatitis virus (VSV). These viruses were selected because human IFIT1 restricts them by
205 distinct mechanisms. VSV, a rhabdovirus with a negative-sense RNA genome, is inhibited by
206 IFIT1 binding to its 5′-triphosphate RNA (5′-ppp-N), which sequesters the genome from the
207 replication pool (2). VEEV TC-83 is inhibited by IFIT1-mediated recognition of its Cap0 RNA,
208 which leads to inhibition of translation (1, 18). IFIT1-expressing cells were infected with an MOI
209 of 1 for both VSV-GFP and VEEV-GFP, and infection was quantified by flow cytometry (Fig 3C).
210 Orthologs that strongly reduced infectivity by at least 70% relative to control cells transduced
211 with an empty lentiviral vector were considered hits. Eleven IFIT1 orthologs (African savannah
212 elephant, Chinese pangolin, sheep, white-tailed deer, black flying fox, dromedary camel, orca,
213 Angola colobus, big brown bat, human, and large flying fox) inhibited VEEV (Fig 3C), and five
214 (orca, cape elephant shrew, dolphin, European rabbit, and nine-banded armadillo) inhibited VSV
215 (Fig 3D). We were surprised that hits for each virus spanned diverse clades with minimal
216 overlap. Only orca IFIT1 restricted both viruses, and just 10 of 39 orthologs met the 70%
217 inhibition threshold, indicating that multiple IFIT1 orthologs target neither VEEV or VSV under
218 these experimental conditions. Western blots revealed wide variation in protein abundance
219 (Supp Fig 2), from high expression (e.g., orca, European rabbit) to very low levels (e.g., African
220 green monkey, greater horseshoe bat). Black-capped squirrel monkey IFIT1 also migrated at a

221 lower-than-expected mass, suggesting a truncation or cleavage of the protein product. However,
222 several low-expressing orthologs were potent restrictors, whereas many highly expressed ones
223 were inactive. These data suggest that IFIT1 orthologs may exhibit species-specific antiviral
224 functions independent of differences in protein expression.

225 We next sought to validate the antiviral phenotypes of a subset of orthologs with more
226 comparable expression. We selected nine orthologs based on protein expression, evolutionary
227 diversity, and variable phenotypes in the screen, including IFIT1 from Chinese pangolin
228 (hereafter referred to as pangolin), orca, sheep, black flying fox, big brown bat, chinchilla,
229 human, chimpanzee, and cape elephant shrew (hereafter referred to as shrew) (Fig 4A). Huh7.5
230 cells were transduced with different doses of lentiviral vectors in an attempt to equalize
231 expression. Western blots showed that eight orthologs were expressed at levels approximately
232 four-fold above to two-fold below human IFIT1. The notable exception was orca IFIT1, which
233 was expressed approximately 15 times higher than human IFIT1 (Fig 4B). IFIT1-expressing
234 cells were challenged with VEEV (Fig 4C) or VSV (Fig 4D) at an MOI of two. VSV was potently
235 inhibited by orca and shrew IFIT1, while no other tested orthologs significantly suppressed
236 infection. Thus, VSV may evade suppression by many mammalian IFIT1s. VEEV was potently
237 inhibited by pangolin, sheep, black flying fox, big brown bat, and human IFIT1, while orca IFIT1
238 was modestly inhibitory. VEEV was not significantly inhibited by chimpanzee IFIT1 but was
239 suppressed by human IFIT1. This was particularly noteworthy as human and chimpanzee IFIT1
240 protein sequences differ by only eight amino acids, and one of these (residue 366) was
241 identified as rapidly evolving by both FUBAR and MEME (Fig 1D). Together, these validation
242 experiments demonstrate that mammalian IFIT1 exhibits species-specific differences in viral
243 suppression. Furthermore, while expression differences in IFIT1 orthologs are noted and may
244 affect antiviral potency, our data suggest that species-specific differences cannot be fully
245 explained by expression differences. This is exemplified by potent restriction of VEEV by

246 pangolin and big brown bat IFIT1 despite low expression (Fig 4B and 4C). Further, high-
247 expressing sheep IFIT1 only restricted VEEV infection, but not VSV, and orca IFIT1 only
248 modestly reduced VEEV infection despite much higher expression than all other IFIT1s (Fig 4B-
249 D).

250 We next tested this subset of nine IFIT1 orthologs against human parainfluenza virus
251 type 3 (PIV3). PIV3 is a paramyxovirus that, like the rhabdovirus VSV, has a negative-sense
252 single-stranded RNA genome, allowing us to compare each ortholog's activity against two
253 viruses that share a replication strategy. We also selected PIV3 because published reports differ
254 on its susceptibility to human IFIT1, whereas the related PIV5 is consistently IFIT1-sensitive
255 (19-22). PIV3 was significantly restricted by shrew, pangolin, chinchilla, black flying fox, and big
256 brown bat IFIT1 (Fig 4E). Suppression of PIV3 by human IFIT1 in our assay was very modest
257 and not statistically significant. Chinchilla IFIT1 exhibited disparate activities, as it did not inhibit
258 VEEV (Fig 4C) or VSV (Fig 4D), yet significantly protected cells from PIV3 infection (Fig 4E).
259 We then tested these IFIT1 orthologs against another alphavirus related to VEEV, Sindbis virus
260 (SINV) (Fig 4E). SINV was largely resistant to most mammalian IFIT1s, consistent with previous
261 human IFIT1 studies (1, 18). However, SINV was potently suppressed by orca IFIT1, and
262 significantly suppressed by pangolin, sheep, and chinchilla IFIT1 (Fig 4E), highlighting a pattern
263 of suppression that was distinct across the nine orthologs relative to the alphavirus VEEV.
264 Together, these data demonstrate that IFIT1 orthologs exhibit a range of antiviral phenotypes
265 with a panel of genetically diverse viruses (Fig 4G), largely independent of differences in protein
266 expression.

267 *Human, black flying fox, and chimpanzee IFIT1 protein exhibit species-specific RNA binding*

268 Human and black flying fox IFIT1 inhibited VEEV, whereas chimpanzee IFIT1 did not
269 (Fig 4C). The black flying fox (*Pteropus alecto*) is a model megabat species that is a reservoir

270 for zoonotic viruses (23-25) and expresses restriction factors with unique antiviral activities (12,
271 26-31). While human and black flying fox IFIT1 share only 69% identity, human and chimpanzee
272 IFIT1 are over 98% identical (Fig 3B, Supp Table 1). The unique phenotypes of these three
273 species, combined with their well annotated genomes and the ease of purifying IFIT1 in
274 bacteria, prompted us to use them for biochemical studies to examine potential differences in
275 their RNA-binding ability.

276 Recombinant IFIT1 proteins (Supp Fig 3) were tested for Cap0 RNA binding by
277 electrophoretic mobility shift assay (EMSA). A 41-nt transcript corresponding to the VEEV 5′
278 UTR was capped with faustovirus capping enzyme to generate RNAs that resemble physiologic
279 Cap0 termini (32). After incubation with purified IFIT1 orthologs, protein–RNA complexes were
280 resolved by native PAGE and visualized (Fig 5A). Quantification of band shift intensity and area
281 under the curve analysis revealed that black flying fox IFIT1 exhibited the strongest RNA binding
282 activity, followed by human IFIT1 (Fig 5B, 5C). Little binding was observed by chimpanzee
283 IFIT1, as band shift intensity was barely above that of a human RNA-binding deficient control
284 (human IFIT1-R187H) (2, 3) (Fig 5B, 5C). These biochemical data are consistent with viral
285 phenotypes (Fig 4C), suggesting that species-specific antiviral activities of IFIT1s can be partly
286 explained by RNA binding potential.

287 *Mutagenesis of primate IFIT1 reveals genetic determinants of IFIT1 antiviral function*

288 Human IFIT1 restricts VEEV and binds its Cap0 RNA, whereas chimpanzee IFIT1 shows
289 no VEEV inhibition and little VEEV Cap0 RNA binding. The two proteins differ at only eight
290 residues (Fig 6A). We therefore used site-directed mutagenesis to pinpoint which substitutions
291 account for this functional gap. Because three of the eight variant residues—362, 364, and
292 366—clustered together (Fig 6A), we created reciprocal “362/4/6” triple-mutant IFIT1 constructs
293 that swap these positions between chimpanzee and human proteins. One of these (human

294 L366, chimpanzee M366) shows positive selection in two computational models (Fig 1D),
295 implying that evolutionary pressure may have shaped the functional divergence between these
296 primate IFIT1 orthologs.

297 Huh7.5 cells expressing wild type (WT) or mutant IFIT1 were challenged with VEEV-
298 GFP at an MOI of two, and infectivity was quantified by flow cytometry (Fig 6B). Western blotting
299 demonstrated near uniform expression of all IFIT1 proteins (Fig 6B). WT chimpanzee IFIT1
300 conferred little protection (approximately 50% infection versus 60% in empty-vector controls),
301 whereas WT human IFIT1 reduced infection to less than 10%. In the human background, only
302 the L366M substitution caused a significant loss of restriction (approximately 4-fold higher
303 infection than WT). Q364R had a modest, non-significant effect, and the 362/4/6 triple mutant
304 nearly abolished activity. In the chimpanzee background, the reciprocal M366L substitution
305 reduced infection by half, R364Q produced a modest, non-significant gain in antiviral activity,
306 and the 362/4/6 triple mutant suppressed VEEV as effectively as WT human IFIT1. These
307 results show that residues N362, Q364, and L366 are necessary for VEEV restriction by human
308 IFIT1, and that their reciprocal substitution is sufficient to endow chimpanzee IFIT1 with potent
309 antiviral activity.

310 Amino acids 362, 364, and 366 are generally conserved across 20 primate IFIT1
311 sequences (Fig 6C). Residue 366 is typically hydrophobic. Fifteen species, including humans,
312 encode leucine, whereas the other five, including chimpanzee, encode either valine or
313 methionine (Fig 6C). This suggests that leucine at position 366, which is rapidly evolving, might
314 be important for antiviral function in primate IFIT1. Additional support for the importance of L366
315 comes from our findings that the only primate IFIT1, besides those of chimpanzees and
316 humans, which was expressed at appreciable levels during the screen was that of the Angola
317 colobus. This IFIT1 variant also potently inhibited VEEV infection and notably contains a leucine

318 at residue 366, similar to human IFIT1 (Fig 3C, Supp Fig 2, Supp Table 1). Glutamine is
319 conserved at site 364 in all primate species aligned except chimpanzee, which encodes an
320 arginine (Q364R) and introduces a positive charge. Point mutants of residue 364 in chimpanzee
321 and human IFIT1 exhibited moderate alterations in anti-VEEV function, though not statistically
322 significant, suggesting that this amino acid may have a minor role in antiviral restriction that
323 synergizes with L366.

324 To test combined effects of residues 364 and 366, double mutants (referred to as 364/6
325 double mut) for both chimpanzee and human IFIT1 were generated. Huh7.5 cells expressing
326 WT, 364/6 double mut, or 362/4/6 triple mut IFIT1s of both chimpanzee and human IFIT1 were
327 challenged with VEEV-GFP at an MOI of two, and infection was quantified by flow cytometry
328 (Fig 6D). Western blotting demonstrated uniform expression of all human and chimpanzee IFIT1
329 mutants (Fig 6D). As in previous experiments, wild-type human IFIT1 strongly suppressed
330 VEEV infection whereas wild-type chimpanzee IFIT1 did not (Fig 6D). However, the 364/6
331 double mut and 362/4/6 triple mut of human IFIT1 both had a near complete loss of antiviral
332 capacity (Fig 6D). These results suggest that residues 364 and 366, but not 362, in human
333 IFIT1 are necessary to confer anti-VEEV function. In contrast, the 364/6 double mutant or the
334 362/4/6 triple mutant of chimpanzee IFIT1 potently suppressed VEEV infection similar WT
335 human IFIT1. No difference in antiviral potency was observed between chimpanzee IFIT1 with
336 the 364/6 double mut or 362/4/6 triple mut, suggesting again that residue 362 does not play a
337 key role in the differential antiviral properties of human and chimpanzee IFIT1. Together, these
338 data indicate that out of eight amino acids that differ between human and chimpanzee IFIT1,
339 sites 364 and 366, in combination, comprise the underlying differences in anti-VEEV function.

340 We next examined the location of amino acids 364 and 366 in the solved crystal
341 structure of human IFIT1 bound to RNA and in the chimpanzee IFIT1 structure predicted by

342 AlphaFold. Residues 364 and 366 are located within the α-helix 18 within TPR7 of IFIT1 (Fig
343 6A, 6E). They are not predicted to contact RNA and are not located in direct proximity of the
344 RNA-binding pocket (Fig 6E, 6F), suggesting they may regulate primate IFIT1 function in an
345 allosteric manner.

346 **Discussion**

347 Here, combining evolutionary and functional data, we conclude that mammalian IFIT1s
348 are rapidly evolving viral restriction factors that exhibit species-specific antiviral activity.
349 Differential antiviral activity of human and chimpanzee IFIT1 led to the unexpected discovery
350 that two residues, 364 and 366, in α-helices 18 within the TPR7 domain of IFIT1 may partially
351 determine primate IFIT1 antiviral capacity. The structures of human and chimp IFIT1 suggest
352 that these amino acids are not directly involved in RNA binding. Thus, they may be involved in
353 conformational changes of IFIT1 during RNA-binding or other allosteric effects that result in a
354 natural loss of function, though additional studies are needed to test this.

355 Our data also support a model in which the breadth of IFIT1 antiviral phenotypes may
356 be, at least partially, explained by differences in RNA-binding ability. VEEV infection was most
357 potently suppressed by black flying fox IFIT1, significantly inhibited by human IFIT1, and
358 unaffected by chimpanzee IFIT1 (Fig 4C). This trend was similarly observed in RNA binding
359 assays with a sequence identical to that of the Cap0 VEEV 5' UTR (Fig 5). These data are
360 consistent with previous studies showing that the ability of IFIT1 to bind viral RNA is required for
361 its antiviral function (4, 33).

362 The differential antiviral activity between IFIT1B and IFIT1 across several mammals was
363 previously demonstrated by Daugherty et al.(11). This study used phylogenetic approaches to
364 show that gene birth, gene loss and gene conversion occurred throughout
365 vertebrate *IFIT* genes, resulting in extensive genetic diversity (11). Furthermore, through viral

366 infection assays and a yeast growth assay, the authors showed different RNA-binding properties
367 and disparate antiviral functions between IFIT1 or IFIT1B proteins from primates, mouse, and
368 cat (11). Our studies significantly expand the diversity of mammalian IFIT1s interrogated for
369 antiviral function. Notably, IFIT1s across *Mammalia* are not universally antiviral against VEEV
370 and VSV. In fact, antiviral specificity of IFIT1 orthologs is possibly quite narrow and highly
371 dependent on which virus is being evaluated.

372 We further show that mammalian IFIT1s spanning diverse orders are rapidly evolving,
373 and that in primates, this is occurring at functionally relevant sites that are not directly implicated
374 in RNA binding. Computational studies identified amino acid 193 in TPR4 loop as rapidly
375 evolving, and scanning mutagenesis showed that this residue is mutationally resilient. This was
376 similarly observed for TRIM5α, in which most mutations within the v1 loop did not affect antiviral
377 potency (34). Alteration of charge within the v1 loop of TRIM5α did play a significant role in
378 determining the antiviral outcome of TRIM5α mutants (34). Similarly, introduction of negatively
379 charged residues at position 193 of human IFIT1 ablated antiviral activity (Fig 2D). Thus,
380 alteration of this single amino acid within IFIT1 may not result in major gain or loss antiviral
381 function, which may maximize the potential for adaptation during evolutionary arms races with
382 viruses. However, we cannot rule out that substitutions at position 193 may influence antiviral
383 function when combined with changes at other sites in IFIT1. Position 193 is also under
384 selection in bats, and multiple codons within or adjacent to the TPR4 loop register as positively
385 selected across all clades examined (Fig 1A-C). Systematic mutagenesis of these residues—
386 alone and in combination—will clarify whether specific side chains or overall loop charge drive
387 species-specific antiviral outcomes.

388 We note several limitations of our study. [1] All IFIT1 ortholog screens were performed by
389 expressing IFIT1 from distinct species in human cells, which may affect natural antiviral

390 function. For example, some IFIT1 orthologs may bind viral RNA, but not interface with human
391 proteins to effectively suppress translation, resulting in no antiviral activity when expressed in
392 human cells. [2] Our experiments focus on expression of IFIT1 alone, without co-expression of
393 other IFIT proteins. As human IFIT1 antiviral activity and RNA-binding is enhanced by
394 interactions with other IFITs (35, 36), it is possible that the activity of IFIT1 orthologs used in this
395 study is also modulated by co-expression with other IFITs from the cognate species. In
396 particular, human IFIT3 modulates IFIT1 Cap0 RNA-binding and antiviral activity (37).
397 Therefore, future experiments testing the antiviral potential of co-expressed IFITs from diverse
398 species would be informative. [3] Our biochemical assays focus on IFIT1 binding to Cap0 RNA
399 only. This is due to comparative studies that have demonstrated IFIT1 has the strongest affinity
400 for Cap0 RNA when compared to other RNAs, such as ppp-RNA (3). This allowed us to use
401 human IFIT1 as a positive control for Cap0 RNA-binding with a strong signal-to-noise for
402 comparison to other IFIT1 orthologs. However, it is possible that differences in ppp-RNA binding
403 may underlie differences in the antiviral potency of IFIT1 towards viruses such as VSV and
404 PIV3. Further, viral RNA secondary structure can affect IFIT binding (1, 21); the capacity of
405 IFIT1 orthologs to bind RNA 5′ termini may therefore vary with tolerance to structure-based
406 occlusion. [4] This study also does not address the possibility that differential viral evasion of
407 IFIT1 proteins contributes to species-specific antiviral activity. In fact, a recent study has
408 identified species-specific sensitivity of IFIT1 proteins to viral evasion factors encoded by
409 poxviruses (38). [5] We have only provided genetic but not biochemical or structural evidence
410 for the underlying differences between chimpanzee and human IFIT1 RNA-binding and antiviral
411 activity. By mutagenesis assays we demonstrate that two amino acid changes confer antiviral
412 activity between chimpanzee and human IFIT1, suggesting a role for residues 364 and 366 in
413 primate IFIT1. Additional insight into the role of these residues might be gained from molecular
414 dynamics simulations using the crystal structure of human IFIT1 bound to Cap0 RNA as a

415 template. It is also possible that these residues in human IFIT1 may be involved in interactions
416 with other proteins, such as IFIT3, which modulates IFIT1 antiviral activity and Cap0 RNA-
417 binding (37). Indeed, subdomain III of IFIT1 (alpha-helices 17-23), which contains residues 364
418 and 366 (part of alpha helix 18), showed partial protection from deuterium uptake by hydrogen-
419 deuterium exchange with mass spectrometry (HDX-MS) during IFIT1-IFIT3 binding experiments
420 (37). However, residues 364 and 366 themselves were not predicted to directly interact with
421 IFIT3, and to date, structural studies have not demonstrated that these residues are directly
422 involved in IFIT1-IFIT3 interactions. Comparisons with the 364/366 double mutant might
423 determine whether these substitutions alter conformational dynamics in a manner that disfavors
424 IFIT1-IFIT3 interaction and/or RNA binding. [6] Our experiments with chimp IFIT1 suggest that
425 amino acid changes at sites 364 and 366 may have resulted in a natural loss of function for this
426 ortholog. However, we only tested four viruses in infection studies and one viral RNA sequence
427 in RNA-binding studies. Therefore, it is possible that chimpanzee IFIT1 inhibits other viruses,
428 such as those that infect chimpanzees in nature. Future studies may also explore this possibility
429 and uncover other amino acid changes that have resulted in IFIT1 loss of function in certain
430 species. Were a loss of IFIT1 function to occur in chimpanzees or other species, this may have
431 also coincided with a gain of dominant antiviral function in another IFIT or complex of IFIT
432 proteins. However, this has yet to be experimentally tested.

433 Summarily, our findings underscore the notion that unbiased screening, investigations of
434 restriction factors from non-model mammalian species, and evolutionary-guided approaches
435 may uncover novel insight into host-pathogen interactions.

436

437 **Materials and Methods**

438 *Cells and cell culture*

439 Huh7.5 and 293T cells (from C. Rice, The Rockefeller University) were maintained in “complete”
440 DMEM: DMEM (Gibco) supplemented with 10% FBS and 1× non-essential amino acids (NEAA;
441 Gibco). All derived stable cells expressing selectable markers were grown in complete DMEM
442 containing puromycin (Gibco; Huh7.5: 4μg/mL). All cells were incubated at 37°C in 5% CO_2. All
443 cell lines have been STR profiled and confirmed negative for mycoplasma contamination by
444 PCR testing (Venor GeM mycoplasma detection kit, Sigma).

445 *Viruses and viral infections*

446 Venezuelan equine encephalitis virus (TC-83 strain) infectious clone was obtained from I.Frolov.
447 VEEV-GFP stocks were generated as previously described (39). Briefly, infectious clone plasmid
448 was linearized, and RNA was in vitro transcribed with the mMESSAGE mMACHINE™ SP6
449 Transcription Kit (Invitrogen) followed by RNA clean-up with the MEGAclear™ Transcription
450 Clean-Up Kit (Invitrogen). BHK-21J cells (8 x 10^6 cells) were then electroporated with 5μg of in
451 vitro transcribed RNA and plated. Media was changed 18 h after plating, and the remaining
452 supernatant was collected 8 h post-media change. After centrifugation to remove cell debris,
453 virus-containing supernatants were aliquoted and stored at -80°C. Sindbis virus (SINV-GFP,
454 clone S300 from M. Heise) (40) was generated as previously described. Vesicular stomatitis
455 virus (VSV-GFP) (from J. Rose) and human parainfluenza virus type 3 (PIV3-GFP) (JS strain,
456 from Peter Collins) were propagated by passaging in BHK-21J cells and storing clarified
457 supernatants as virus stocks at -80°C. All viral infections were performed in DMEM
458 supplemented with 1% FBS and 1x non-essential amino acids at a total volume of 0.2mL in 24-
459 well tissue culture plates. After a 1 h incubation period, 0.3mL of complete DMEM was added to
460 all wells until harvest. For analysis of viral infection by flow cytometry, cells were dissociated
461 from the plate with 150μL Accumax (Innovative Cell Technologies) and then fixed in
462 paraformaldehyde at a final concentration of 1%. Cells were allowed to fix for at least 30 min at

463 4°C and subsequently centrifuged at 1500 x *g* for 5 min. Supernatant was removed from cell
464 pellets and fixed cells were then resuspended in FACS buffer (PBS [Gibco] supplemented with
465 3% FBS). Flow cytometry was performed on the Stratedigm S1000EON benchtop flow
466 cytometer, with analysis in FlowJo software.

467 *Cloning and plasmids*

468 IFIT1 coding sequences were obtained from the NCBI database. IFIT1 sequences were cloned
469 into the Gateway expression vector pSCRPSY (41). IFIT1 orthologs were synthesized as
470 gBlocks (IDT) with Gateway compatible DNA sequences and an N-terminal HA tag. Human and
471 chimpanzee IFIT1 point mutants were generated using site-directed mutagenesis PCR. Human
472 and chimpanzee IFIT1 362/4/6 triple mutants and 364/6 double mutants were generated by
473 Gibson cloning of gBlocks (IDT). For protein purification, IFIT1 protein coding sequences that
474 were codon-optimized for bacterial expression were cloned into a modified pET28a bacterial
475 expression vector, containing an N-terminal 6X-His tag followed by the yeast Sumo (smt3).

476 *Western Blotting*

477 Cells were lysed with M-PER (Mammalian Protein Extraction Reagent, Thermo Scientific)
478 containing 1x complete protease inhibitor cocktail (Roche) at 4°C for 5 min with intermittent
479 rocking. Lysate was then stored at -80°C. For running SDS-PAGE, lysate was thawed on ice,
480 and mixed to a final concentration of 1x SDS Loading Buffer (0.2 M Tris-Cl pH 6.8, 5% SDS,
481 25% Glycerol, 0.025% Bromophenol Blue, and 6.25% beta-mercaptoethanol). Samples were
482 run on 12% TGX FastCast acrylamide gels (Bio-Rad) or 4-20% Mini-PROTEAN® TGX™
483 precast protein gels (BioRad) and transferred to nitrocellulose membranes using a TransBlot
484 Turbo system (Bio-Rad). Membranes were blocked with 5% milk in 1x Tris Buffered Saline, with
485 Tween-20 (TBS-T [20mM Tris, 150mM NaCl, 0.1% Tween-20]) for at least 45min. Subsequent
486 incubation with primary antibody (at dilutions between 1:500 to 1:5000) diluted in 1% milk in

487 TBS-T was performed overnight, rocking at 4°C. Primary antibodies probing for GAPDH
488 (Proteintech Cat# 10494-1-AP, RRID:AB_2263076 or Proteintech Cat# 60004-1-Ig,
489 RRID:AB_2107436), IFIT1 (Proteintech Cat# 23247-1-AP, RRID:AB_2811269) and HA-tagged
490 IFIT1 (Biolegend Cat# 901502, RRID:AB_2565006) were used in this study. After incubation
491 with primary antibodies, membranes were washed 3 times with TBS-T by rocking for 5 min.
492 Secondary antibodies (Goat anti-Rabbit 800CW and Goat anti-Mouse 680RD [LI-COR] at
493 1:5000 dilutions) diluted in 1x TBS-T were incubated with membranes for at least 45 min.
494 Membranes were then washed 3 times with TBS-T by rocking for 5 min. Proteins were
495 visualized using the LI-COR Odyssey FC imaging system.

496 *Lentivirus production and transduction*

497 To generate lentivirus pseudoparticles, 350,000 293Ts were plated onto poly-lysine coated 6-
498 well plates. Lentiviral packaging plasmids expressing VSV-g and Gag-pol were then mixed with
499 SCRPSY plasmids at a ratio of 0.1µg:0.5 µg:2.5 µg, respectively. Plasmids were incubated for
500 20 min with a mix of XtremeGENE9 transfection reagent (Roche) and OptiMEM (Gibco).
501 Transfection complexes were then added to 293T cells in 1mL of DMEM supplemented with 3%
502 FBS dropwise. After 6 h of incubation, media was changed to 1.5 mL of DMEM supplemented
503 with 3% FBS. Supernatants containing lentiviral pseudoparticles were harvested at 48 and 72 h
504 post-transfection. Lentiviral pseudoparticles were then processed by adding 4µg/mL Polybrene
505 (Sigma), 20mM HEPES, centrifuging at 1500rpm for 5min to remove cell debris, and storing at -
506 80°C until transductions.

507 Lentivirus transductions were performed in 6-well plates after plating 350,000 cells (Huh7.5).
508 Final volume of transductions was either 1mL or 1.5mL of lentivirus mixed with “pseudoparticle”
509 DMEM (DMEM supplemented with 3% FBS, 4µg/mL Polybrene, and 20mM HEPES) After a 6 h
510 incubation at 37°C, 2mL of complete DMEM was added to all transductions. Transduced cells

511 were split into selection media 48h post-transduction and passaged for a minimum of three
512 passages in selection media.

513

514 *Protein Purification*

515 IFIT1 protein coding sequences that were codon-optimized for bacterial expression were cloned
516 into a modified pET28a bacterial expression vector, containing an N-terminal 6X-His tag
517 followed by the yeast Sumo (smt3). Plasmids were transformed into Rosetta DE3 cells.
518 Transformants were grown in Terrific Broth (TB) with 50 mg/L Kanamycin and 34 mg/L of
519 Chloramphenicol and Antifoam B at 37 °C. At the OD_{600} of 0.4, the temperature was lowered to
520 18 °C. Protein expression was induced at OD_{600}=3 by addition of IPTG to 0.4 mM final
521 concentration. Cells were harvested after an overnight incubation by centrifugation (OD_{600}=~8.5)
522 and lysed in the lysis buffer (50 mM Tris-HCl pH 8, 500 mM NaCl, 15 mM Imidazole, 1 mM
523 PMSF, 4 mM β-ME) by sonication. Cell lysates were cleared by centrifugation at 35,000 x g for
524 30 minutes. The cleared lysate was applied onto a gravity column with pre-washed Ni-NTA
525 resin. Resin was washed with 50 mM Tris-HCl pH 8, 1 M NaCl, 30 mM Imidazole, 4 mM β-ME.
526 Proteins were eluted with 50 mM Tris-HCl pH 8, 300 mM NaCl, 300 mM Imidazole, 2 mM DTT.
527 Proteins were treated with Ulp1 protease overnight to remove the Sumo tag and passed over a
528 size-exclusion column (HiLoad 16/600 Superdex 200 pg), equilibrated with 50 mM Tris 8.0, 150
529 mM NaCl, 1 mM DTT. Peak fractions were pooled, concentrated by ultrafiltration, and stored at -
530 80 °C until use. For SDS-PAGE gels of purified IFIT1 protein, 500nM of human, black flying fox,
531 chimpanzee, and human R187H mutant IFIT1 were boiled in 4X Laemmli Sample Buffer
532 (BioRad) with 1.25% BME and loaded into a 4-20% Mini-PROTEAN® TGX™ Precast Protein
533 Gel (BioRad). Gels were run and subsequently incubated in Coomassie stain (40% ethanol,
534 10% glacial acetic acid, 0.1% Coomassie R-250) for 1 hour and destained overnight (10%

535 ethanol, 7.5% glacial acetic acid). Gels were imaged with the ChemiDoc Imaging System
536 (BioRad).

537 *RNA Electrophoretic mobility shift assay*

538 Protein stock concentration of IFIT1 orthologs was determined by diluting protein 1:5 in 1x TBE
539 and measuring A280. Extinction coefficient was determined by ProtParam tool (Expasy), and
540 subsequently used to calculate and normalize protein concentrations between stocks.

541 Before loading, native gels (10% 19:1 Acrylamide: Bis-acrylamide, 25mM NaCl, 1x TBE,
542 0.0005% APS, 0.001% TEMED) were pre-run with 1x TBE in a cold room for at least 2.5 h.
543 While gels were pre-running, binding reactions were set up at room temperature after thawing
544 and keeping both RNA and protein stocks on ice. All dilutions of protein and RNA were in 1x
545 reaction buffer (50nM TRIS pH 8.0, 100mM NaCl, 1mM EDTA, 0.01mg/mL Heparin sodium
546 sulfate, 2.5% Glycerol). For binding reactions, 50nM of Cap0 RNA was mixed 1:1 with 0, 80,
547 160, 240, 320, and 400nM of purified IFIT1 protein in a final volume of 20µL and incubated at
548 room temperature for 20 min.

549 18 µL of RNA:Protein complexes were then run on pre-run native gels for 2.5 h at 100V in 1x
550 TBE in a cold room. Gels were then stained with 1x SYBR Gold stain (ThermoFisher Scientific)
551 diluted in 1x TBE for 20 min rocking at room temperature and imaged on a ChemiDoc Imaging
552 System (BioRad) with UV transillumination. Band intensity was subsequently analyzed using
553 ImageLab software (BioRad).

554 *In vitro transcription and 5' capping of RNA probes*

555 Uncapped RNA probes were generated using the T7 RiboMAX™ Express Large Scale RNA
556 Production System (Promega). Manufacturer instructions were modified for generating short
557 RNA probes. Briefly, 10µM of DNA oligos corresponding to the T7φ2.5 promoter sequence and

558 the complementary T7φ2.5 promoter sequence followed by the first 41nt of the VEEV TC-83
559 strain 5' UTR sequence. Oligos were boiled at 95°C for 2-3 min and then slow cooled to room
560 temperature to allow annealing. 1 μM of the annealed DNA oligos served as the template per
561 20μL T7 transcription reaction. RNA was purified according to manufacturer instructions using
562 phenol:chloroform nucleic acid extraction (Promega).

563 To generate Cap0 RNA, purified uncapped RNA probes were modified using the Faustovirus
564 Capping Enzyme (FCE) (NEB) using modified manufacturer instructions. Briefly, 100μL
565 reactions were composed of 20μL of uncapped RNA purified after T7 transcription (described
566 above), 0.2mM SAM, 1mM GTP, 7500U of FCE, 1x FCE reaction buffer, 80U RNasin® Plus
567 Ribonuclease Inhibitor (Promega), and nuclease-free water up to 100μL. Reactions were
568 incubated at 42°C for 4.5 h and then another 0.5 h at 50°C. Cap0 RNA was then purified using
569 the same phenol:chloroform nucleic acid extraction as performed after the T7 transcription
570 reaction (Promega). Cap0 RNA was determined to be at least 95% Cap0 RNA (m7GpppA) by
571 targeted LC/MS after Nuclease P1 (NEB) digestion at 37°C for 30 min followed by inactivation of
572 enzyme at 95°C for 2 min. LC/MS was performed by the UT Southwestern Preclinical
573 Pharmacology Core Facility.

574

575 *Computational Evolutionary Analysis*

576 IFIT1 coding sequences for all analyses were obtained from the NCBI database. Alignment of
577 multiple sequences was performed using MUSCLE and ClustalW implemented in MEGA X (42).
578 Maximum-likelihood trees were constructed in MEGA X, with standard settings. Trimmed
579 alignments were then generated (43), and when required, ALTER (44) was used to convert file
580 formats. MEME (45) and FUBAR (14) were performed with HyPhy (46) using the Datamonkey
581 web application (47). To perform PAML analysis, we used default settings with the F3x4 codon

frequency table within CodeML. Likelihood ratio tests were performed to compare model 7 versus model 8 and model 8 versus model 8a to determine the presence of positive selection. Bayes empirical Bayes testing was performed to determine specific residues that are adaptively evolving. To detect potential recombination in IFIT1, GARD analysis (16) was performed on aligned coding sequences with HyPhy (46) using the Datamonkey web application (47). Recombination Detection Program version 4 (RDP4) (17) was also used to remove inferred recombinant sequences from alignment, using default settings. Maximum likelihood tree comparing IFIT1, IFIT1B, and IFIT3 C-terminal sequences was aligned using MUSCLE in MEGA X, followed by maximum likelihood tree generation with 1000 bootstrap replicates in MEGA X (42). Alignment to the C-terminal region of IFITs to distinguish IFIT1 and IFIT1B sequences was previously described (11). Species trees were generated using the TimeTree database (48). FigTree software was then used to make trees shown in figures. Alignments and determination of amino acid identity to human IFIT1 was performed using ClustalOmega (49). Graphics comparing human and chimpanzee IFIT1 structures were generated using ChimeraX (50).

Statistical analysis

All statistical analyses were performed in GraphPad Prism 9. All graphs represent the mean of n=3 independent biological replicates with error bars representing standard deviation. ns, $p > 0.05$, *, $p < 0.05$, **, $p < 0.01$, ***, $p < 0.001$, and **** $p < 0.0001$.

Acknowledgements

We thank Adam Osinski and Gina Park in the lab of Vincent Tagliabracci for purifiying IFIT1 protein and for technical assistance with RNA EMSAs. This work was funded in part by the National Science Foundation Graduate Research Fellowship (2019274212 to M.B.M.) and

grants to J.W.S: NIH Grant AI158124, The Welch Foundation (I-2013-20220331), the UT Southwestern High Impact / High Risk Grant, and an Investigator in the Pathogenesis of Infectious Disease Award from the Burroughs Wellcome Fund.

Author Contributions

M.B.M, A.M.D., and E.N. performed technical experiments. M.B.M. and I.N.B. performed computational evolutionary analysis. M.B.M and J.W.S conceptualized this study and designed experiments. M.B.M and J.W.S wrote and edited the manuscript. M.B.M and J.W.S obtained funding.

A

Clade	N	p-value (M7vsM8)	p-value (M8vsM8a)	omega (dN/dS)	Positively selected sites (BEB p>0.95)
Primate	20	0.0006088	0.0002588	0.53606	193, 200
Bat	9	0.000001492	0.000003884	0.58854	193, 196, 367
Carnivore	21	0.008238	0.02007	0.40348	3, 296
Ungulate	21	8.58E-15	3.73E-15	0.88076	28, 44, 194, 195, 196, 197, 198, 203, 245, 284, 302, 319, 321, 325, 329, 339, 370, 372, 407, 411, 417, 474

B

Clade	N	Positively Selected Sites (>0.95 Probability)
Primate	20	30, 170, 193, 240, 366
Bat	9	193
Carnivore	20	N/A
Ungulate	20	196, 325, 417

C

Clade	N	Positively Selected Sites (<0.05 threshold)
Primate	20	2, 136, 170, 251, 266, 366, 414
Bat	9	80, 84, 92, 115, 127, 131, 153, 193, 230, 232, 298, 351, 352, 466
Carnivore	20	3, 7, 11, 63, 322
Ungulate	20	109, 129, 190, 200, 264, 265, 266, 284, 295, 302, 325, 329, 339, 406, 417, 472

D

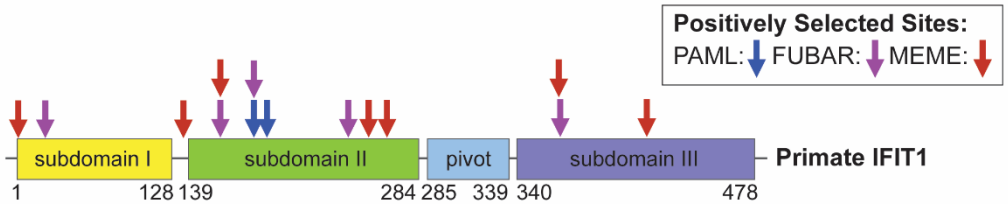

Figure 1. Evolutionary analysis of IFIT1 from clades of mammals reveals rapid evolution. A. PAML analysis on NCBI-derived coding sequences that were aligned and then analyzed using CodeML. Likelihood ratio tests were performed to compare model 7 vs model 8 and model 8 vs model 8a to determine the presence of positive selection. N=number of sequences input, and numbers under "positively selected sites" represent residue number of the reference sequence. B. FUBAR analysis on aligned coding sequences using HyPhy software and DataMonkey. N=number of sequences input, and numbers under "positively selected sites" represent residue number of the reference sequence. C. MEME analysis on aligned coding sequences using HyPhy software and the DataMonkey application. N=number of sequences input, and numbers under "sites of episodic positive selection" represent residue number of the reference sequence. D. Diagram of Primate IFIT1 domains and location of positively selected sites determined by PAML, FUBAR, and MEME.

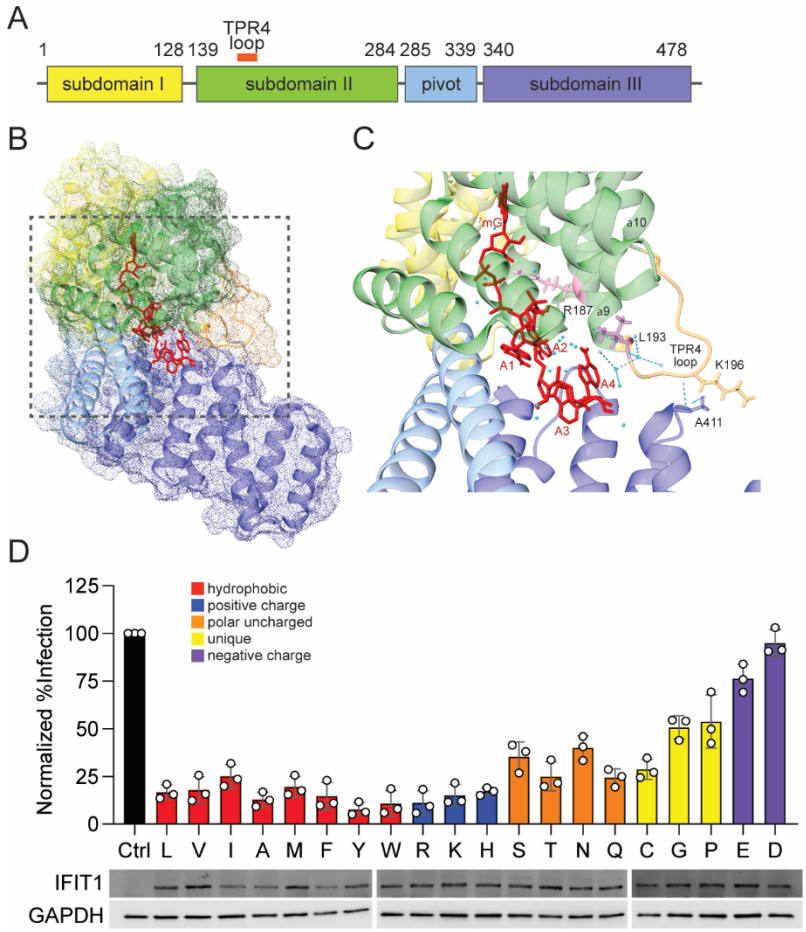

Figure 2. Mutagenesis of rapidly evolving residue 193 in human IFIT1 reveals mutational resiliency. A. Depiction of the human IFIT1 protein with the TPR4 loop location (orange) shown. B. Solved crystal structure of IFIT1 bound to RNA with TPR4 loop forming a “lid” over the exit of the RNA-binding tunnel (PDB:5udj). C. Zoom in on the TPR4 loop and RNA-binding tunnel exit illustrating the location of the TPR4 loop and residue 193 in relation to bound RNA in the human IFIT1 crystal structure. D. (Top) Saturating mutagenesis screen in cells expressing human IFIT1 with residue 193 mutated to every possible residue and challenged with VEEV infection. (Top) (Bottom) Western blot from lysates of Huh7.5 cells expressing IFIT1 point mutants.

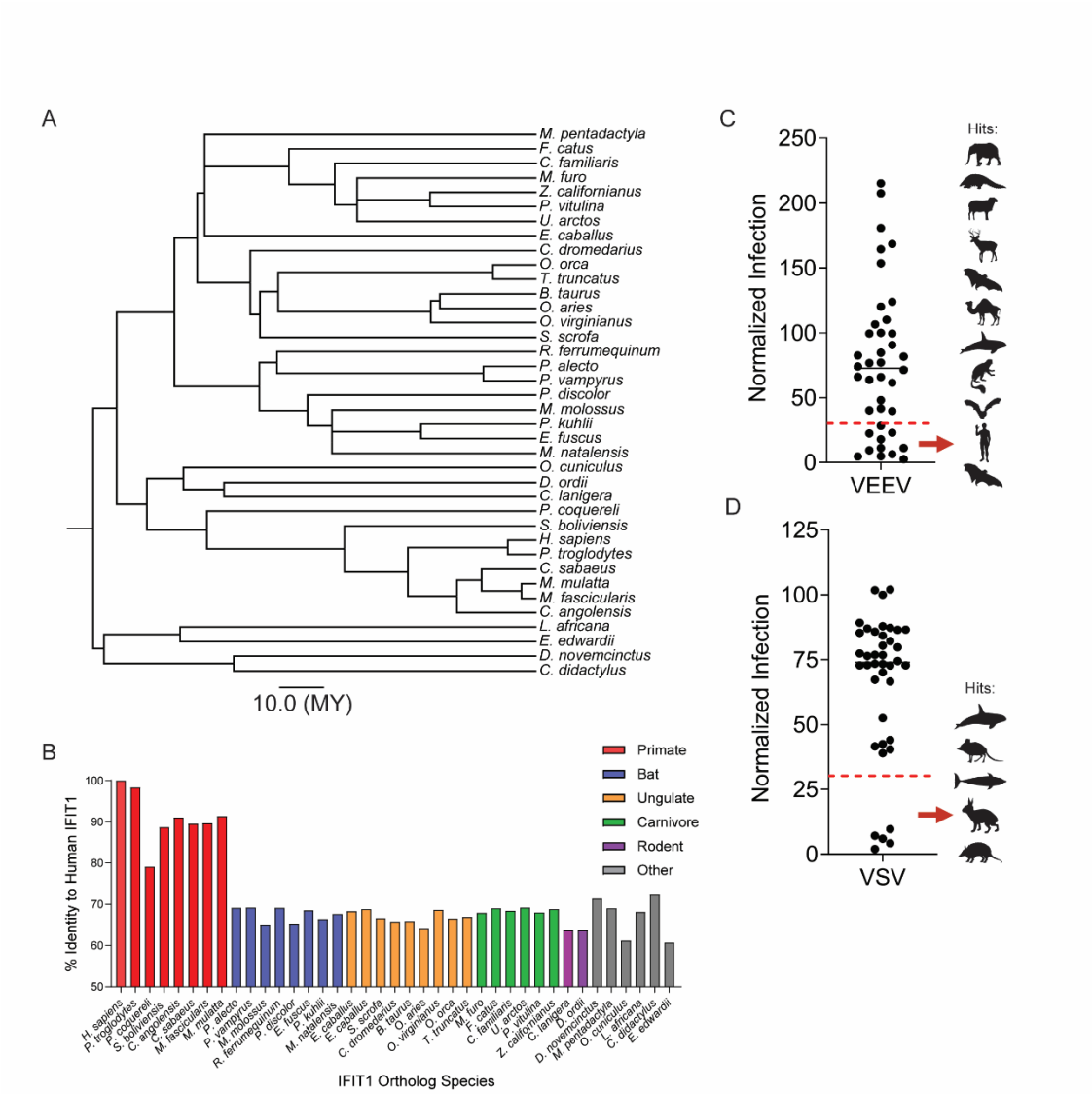

Figure 3. IFIT1 ortholog screens reveal extensive heterogeneity in mammalian IFIT1 antiviral function. A. TimeTree illustrating the evolutionary relationship of IFIT1 orthologs selected for ortholog screen. Scale bar represents divergence time of 10 million years. B. Graph of protein sequence identity of IFIT1 orthologs used in screen relative to human IFIT1. C. Dot plot representing the relative infection (compared to control cells) from an ectopic overexpression screen in which Huh7.5 cells expressing 39 different IFIT1 mammalian orthologs were challenged with 1.0 MOI VEEV-GFP for 4 h. Infectivity was quantified by flow cytometry. Red line denotes 30% relative infection. n=2 independent experiments. D. Same as C, for VSV-GFP (1 MOI, 4 h infection). n=3 independent experiments. In C, D, silhouettes represent the species with a relative inhibition of at least 70% in order from most (top) to least (bottom) inhibitory..

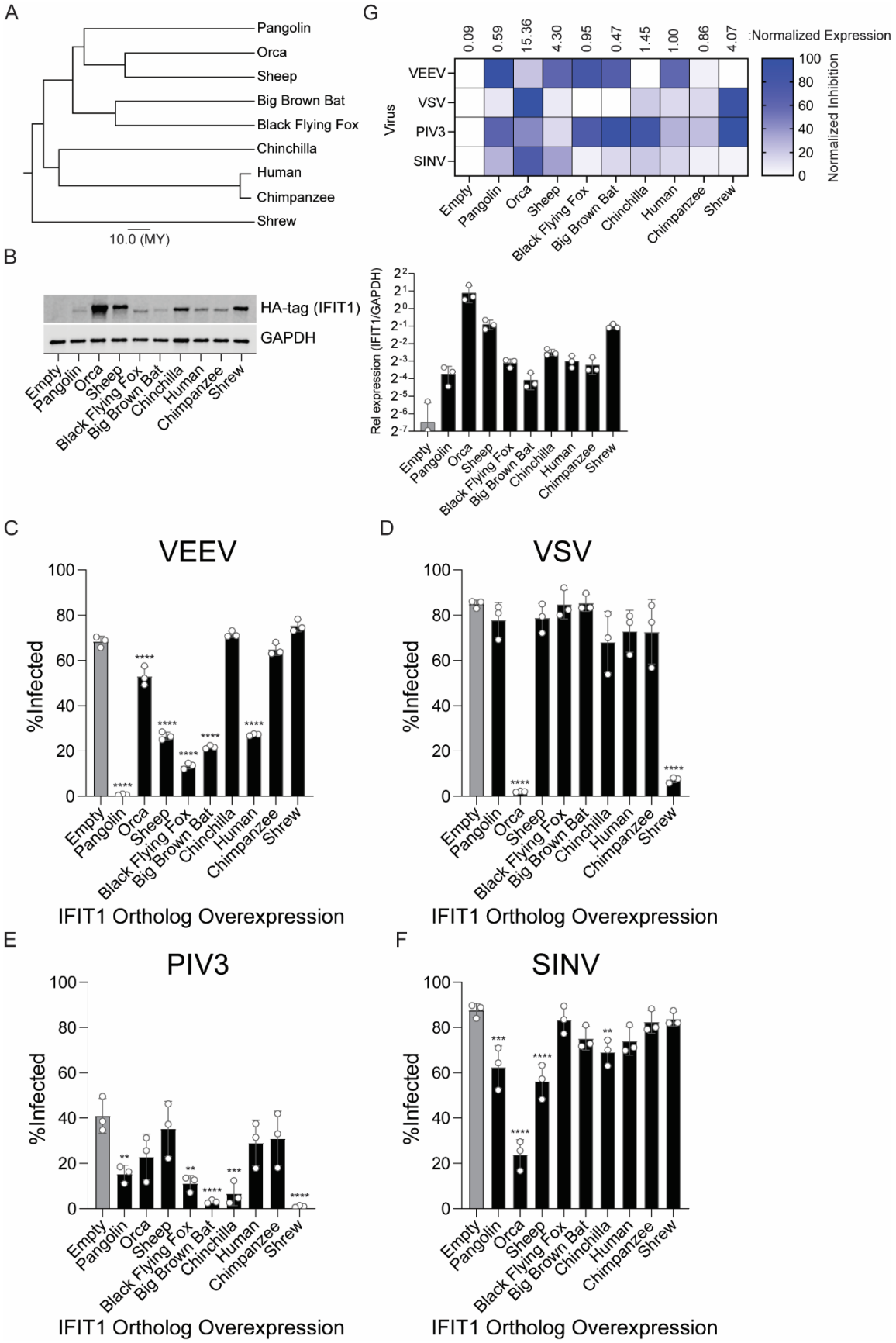
A
Pangolin
Orca
Sheep
Big Brown Bat
Black Flying Fox
Chinchilla
Human
Chimpanzee
Shrew
10.0 (MY)
B
HA-tag (IFIT1)
GAPDH
Empty
Pangolin
Orca
Sheep
Black Flying Fox
Big Brown Bat
Chinchilla
Human
Chimpanzee
Shrew
G
0.09
0.59
15.36
4.30
0.95
0.47
1.45
1.00
0.86
4.07
:Normalized Expression
VEEV
VSV
PIV3
SINV
Virus
Normalized Inhibition
Rel expression (IFIT1/GAPDH)
C
VEEV
%Infected
IFIT1 Ortholog Overexpression
D
VSV
%Infected
IFIT1 Ortholog Overexpression
E
PIV3
%Infected
IFIT1 Ortholog Overexpression
F
SINV
%Infected
IFIT1 Ortholog Overexpression

664

Figure 4. Validation of selected IFIT1s from ortholog screen. A. TimeTree illustrating the evolutionary relationship of IFIT1 orthologs selected for screen validation and follow-up. Scale bar represents divergence time of 10 million years. B. Western blot from cells expressing HA-tagged IFIT1 orthologs used in C-F. Image is representative of three independent replicates. Quantification of band intensity was performed using LiCOR Image Studio C. Infection of IFIT1 ortholog-expressing Huh7.5 cells with VEEV-GFP (MOI 2, 4h) D. Infection of IFIT1 ortholog-expressing Huh7.5 cells with VSV-GFP (MOI 2, 4h) E. Infection of IFIT1 ortholog-expressing Huh7.5 cells with PIV3-GFP (MOI 2, 10h) F. Infection of IFIT1 ortholog-expressing Huh7.5 cells with SINV-GFP (MOI 2, 10h). G. Heat map summarizing the infection data shown in C-F and complementary ortholog expression data shown in B. In C-F, data represent mean ± SD, n=3 independent experiments. Statistical significance was determined by one-way ANOVA with Dunnett's test. ns $p > 0.05$, **$p < 0.01$, ***$p < 0.001$, and ****$p < 0.0001$.

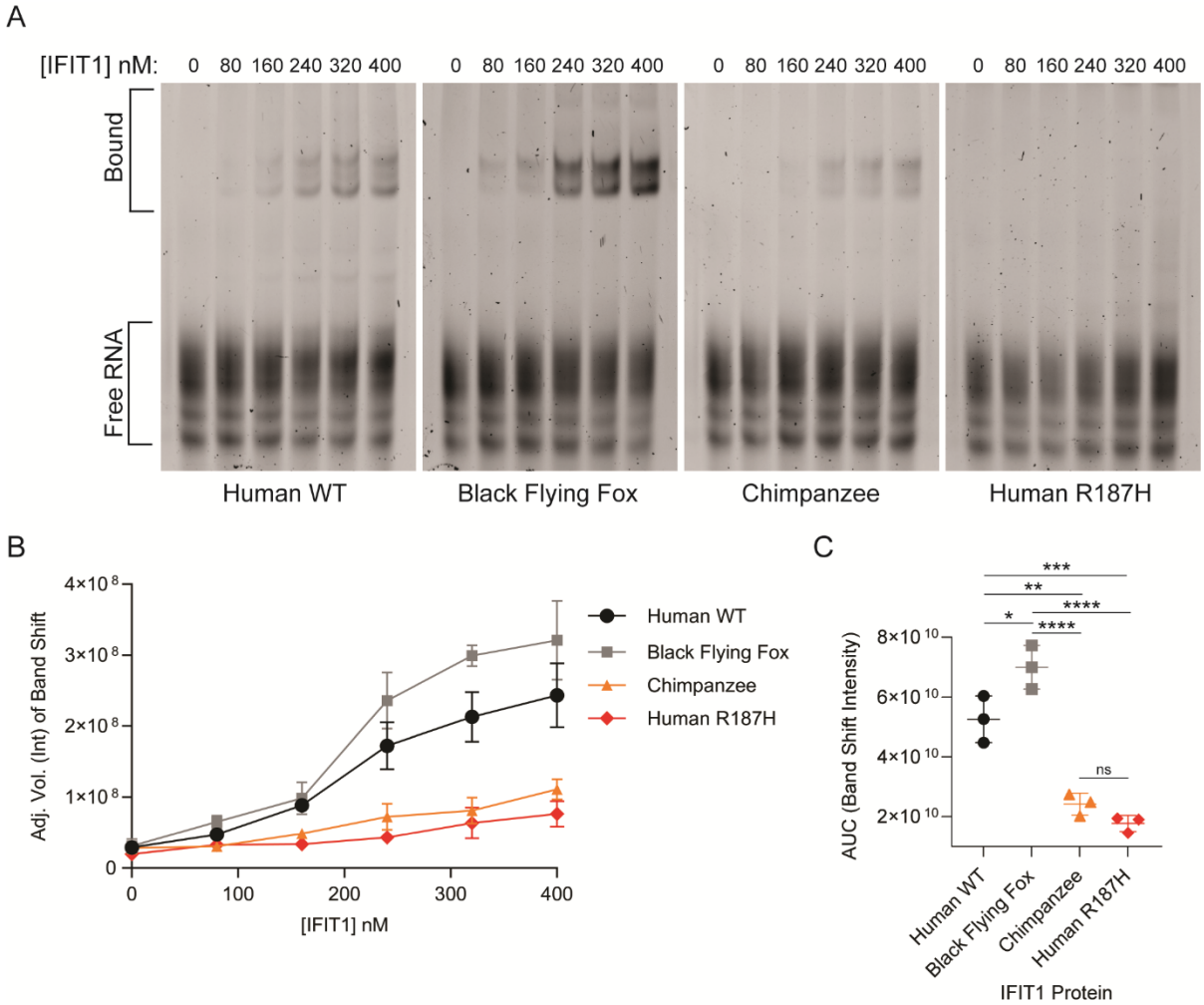

Figure 5. IFIT1 proteins exhibit species-specific Cap0 RNA binding. A. RNA EMSA with Cap0 VEEV RNA probes (41nt of VEEV TC-83 strain 5' UTR) at 50nM incubated with increasing concentrations of the indicated purified IFIT1 proteins. Images are one representative image from three independent replicates. B. Plot of the band shift intensity from EMSAs in A. Data represent mean ± SD, n=3 independent experiments. Band intensity was quantified by ImageLab software (BioRad). C. Area Under the Curve (AUC) analysis calculated from raw data in B. Statistical significance was tested by one-way ANOVA with correction for multiple comparisons. Data represent mean ± SD, n=3 independent experiments. ns, $p > 0.05$, *, $p < 0.05$, **, $p < 0.01$, ***, $p < 0.001$, and **** $p < 0.0001$.

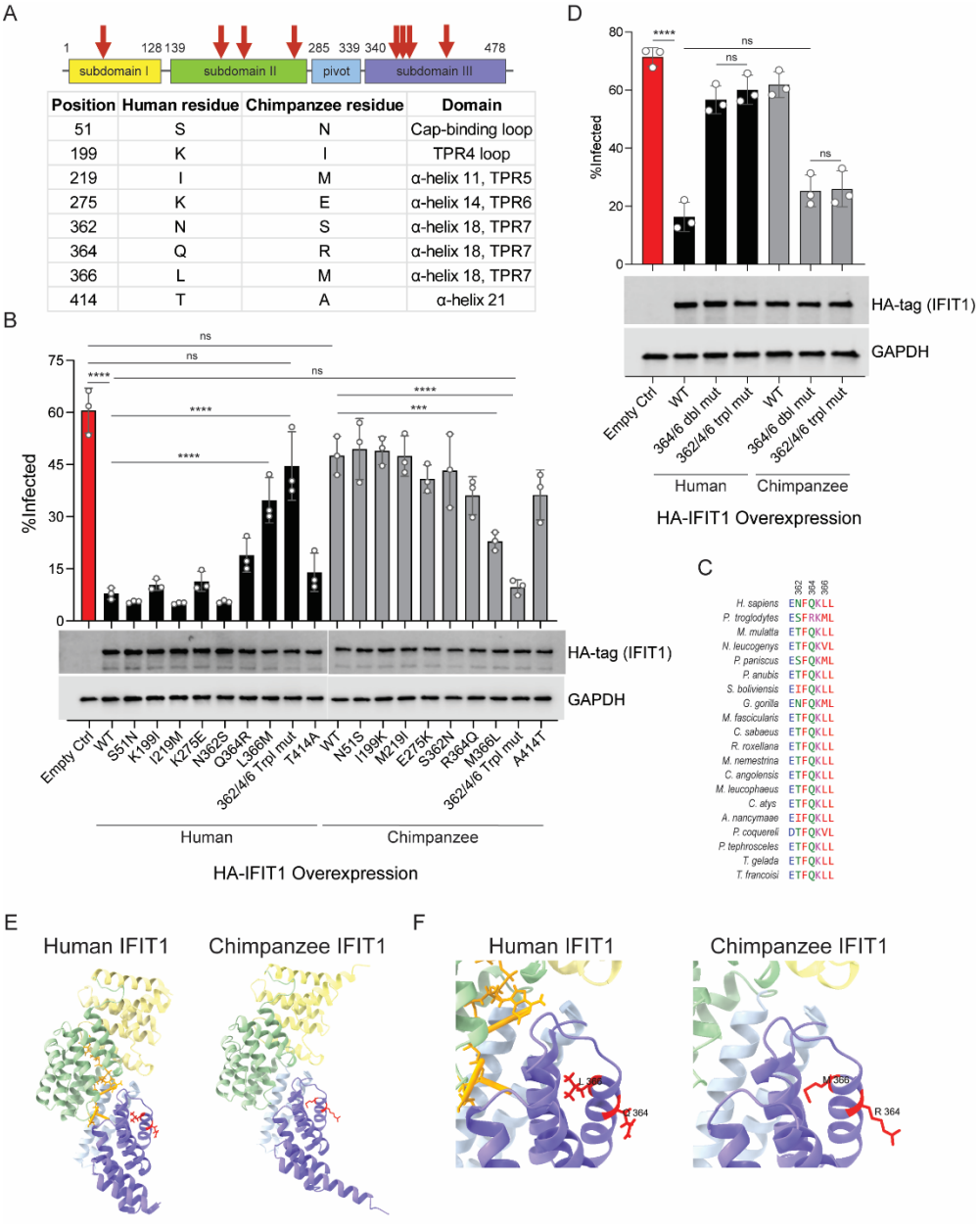

Figure 6. Mutagenesis uncovers genetic determinants of primate IFIT1 antiviral function. A. Diagram and chart describing amino acids that differ between human and chimpanzee IFIT1 as well as their domain location. B. Effects of primate IFIT1 mutant expression on VEEV-GFP infection. Huh7.5 cells were infected with an MOI of 2 for 4 h and infectivity was quantified by flow cytometry. Data represent mean ± SD, n=3 independent experiments. Statistical significance was determined by one-way ANOVA with Dunnett's test. ns, $p > 0.05$; ***, $p < 0.001$; and **** $p < 0.0001$. Western blotting for HA-tag (IFIT1) and GAPDH (Loading control) was also performed to determine expression levels of IFIT1 mutants. C. ClustalOmega protein sequence alignment of residues 361-367 of IFIT1 from 20 primate species. D. Effects of primate IFIT1 double or triple mutants on VEEV-GFP infection. Huh7.5 cells were infected with an MOI of 2 for 4 h and infectivity was quantified by flow cytometry. Data represent mean ± SD, n=3

707 independent experiments. Statistical significance was determined by one-way ANOVA with
708 Dunnett's test. ns, $p > 0.05$; and **** $p < 0.0001$. Western blotting for HA-tag (IFIT1) and
709 GAPDH (Loading control) was also performed to determine relative IFIT1 mutant protein
710 abundance. E. Structure of human IFIT1 bound to RNA (left) or AlphaFold predicted structure of
711 chimpanzee IFIT1 (right) visualizing location of residues 364 and 366 (red) that confer antiviral
712 activity. Graphics were generated using ChimeraX. F. Zoom in of (E).

A

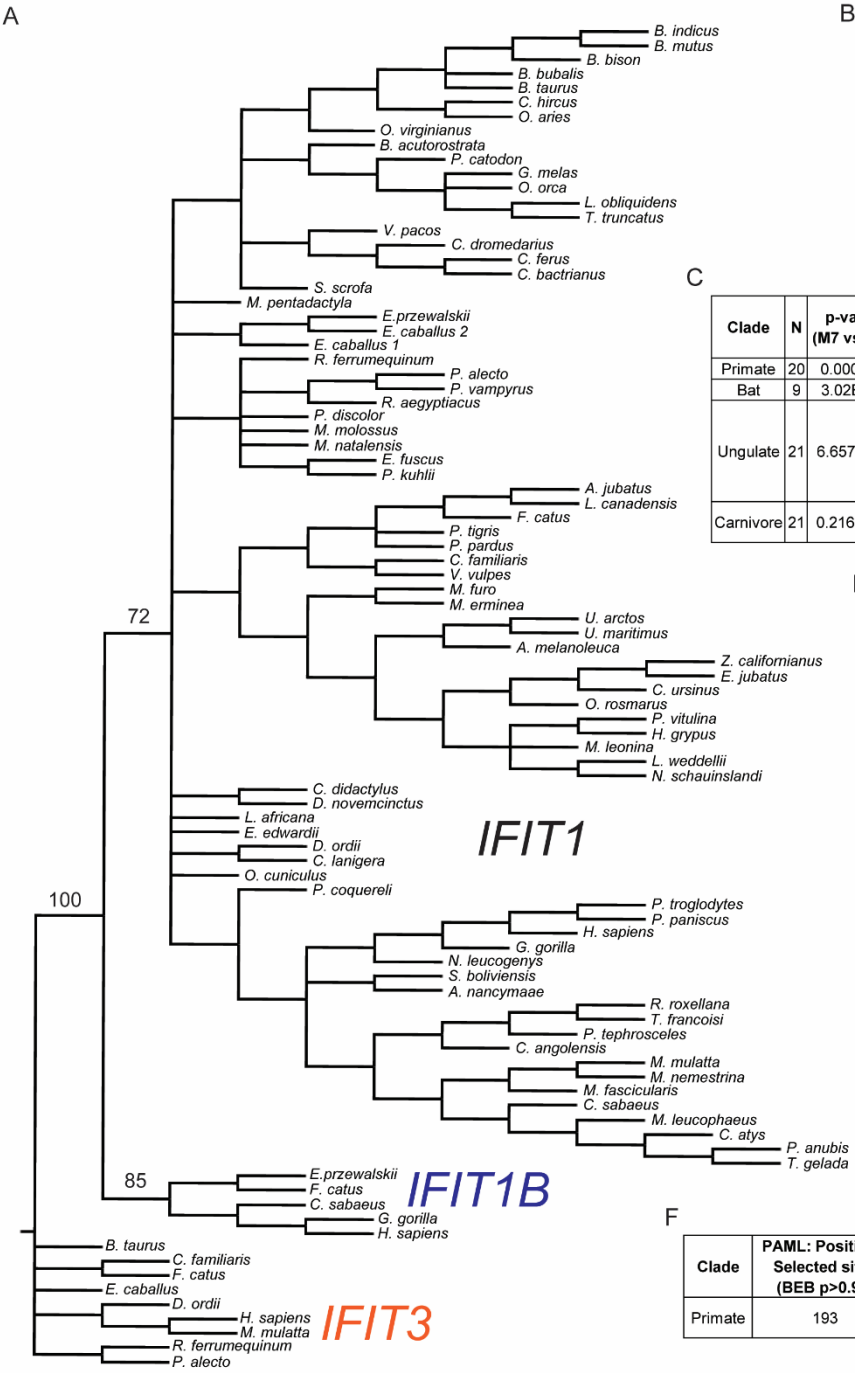

B

Clade	N	# Predicted Breakpoints	Breakpoint Coordinates (bp)
Primate	20	1	113
Bat	9	2	97, 1143
Ungulate	20	1	563
Carnivore	20	2	41, 1109

C

Clade	N	p-value (M7 vs M8)	p-value (M8 vs M8a)	Positively selected sites (BEB p>0.95)	omega (dN/dS)
Primate	20	0.000427	0.00018738	193, 200	0.54901
Bat	9	3.02E-06	1.3105E-05	193, 196, 266, 267	0.57954
Ungulate	21	6.657E-12	1.3266E-12	195, 196, 197, 198, 245, 284, 321, 325, 329, 339, 366, 370, 407, 411, 417, 473, 474	0.96119
Carnivore	21	0.2163716	0.66530435	N/A	0.34721

D

Clade	N	Positively Selected Sites (>0.95 Probability)
Primate	19	170, 193, 197, 240, 366
Bat	9	193
Ungulate	20	325, 417
Carnivore	20	N/A

E

Clade	N	Positively Selected Sites (<0.05 threshold)
Primate	19	170, 230, 251, 266, 366, 414
Bat	9	80, 92, 115, 131, 153, 193, 230, 232, 298, 351, 352
Ungulate	20	190, 200, 264, 265, 266, 284, 302, 325, 329, 339, 406, 407, 417, 472
Carnivore	20	63, 322

F

Clade	PAML: Positively Selected sites (BEB p>0.95)	FUBAR: Positively Selected Sites (>0.95 Probability)	MEME: Positively Selected Sites (<0.05 threshold)
Primate	193	30, 170, 193, 197, 294, 362, 366	170, 199, 251, 266, 366, 414

713

714 **Supplementary Figure 1. Analysis of IFIT1 for recombination and positive selection.** A.
715 Maximum likelihood tree of C-terminal region of IFIT1, IFIT1B, and IFIT3 coding sequences
716 (corresponding to bases 907-1437 of human IFIT1 coding sequence), generated in MEGA X
717 with 1000 bootstrapping replicates. Select bootstrap values are shown. B. GARD analysis of
718 IFIT1 coding sequences used for evolutionary analysis in Figure 1. C. PAML analysis on regions
719 of IFIT1 coding sequence after (primate and ungulate) or between (bat and carnivore)
720 breakpoints indicated in B. D. FUBAR analysis on regions of IFIT1 coding sequence after
721 (primate and ungulate) or between (bat and carnivore) breakpoints indicated in B. E. MEME
722 analysis on regions of IFIT1 coding sequence after (primate and ungulate) or between (bat and
723 carnivore) breakpoints indicated in B. F. PAML, FUBAR, and MEME analysis on primate IFIT1
724 coding sequence after removal of inferred recombinant sequences by Recombination Detection
725 Program 4 (RDP4).

726

A

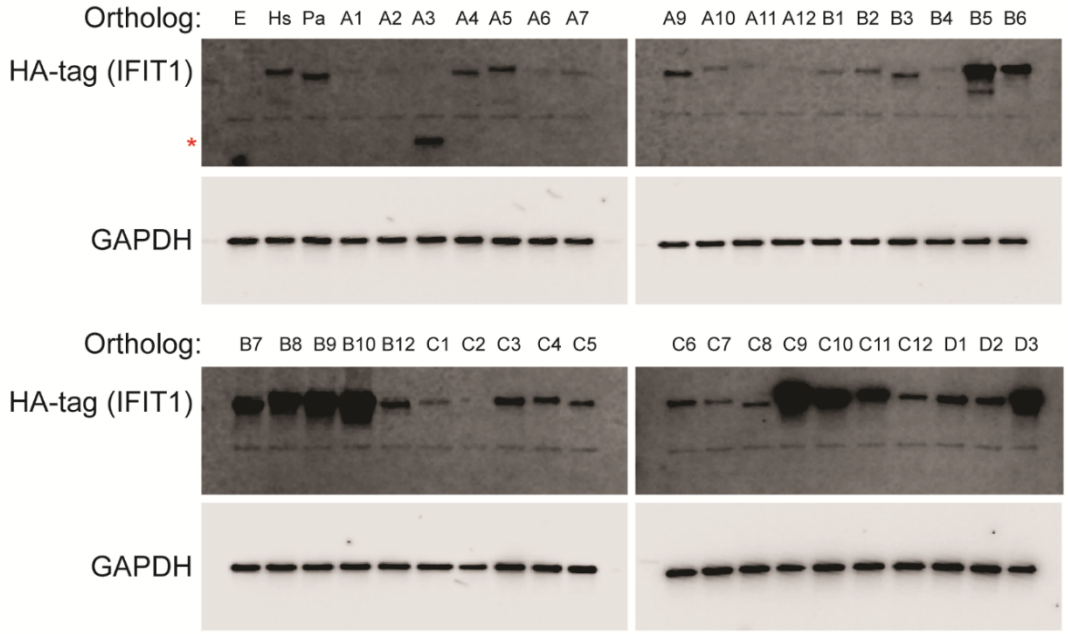

B

Common Name	Scientific Name	Key	Common Name	Scientific Name	Key
Empty Control	N/A	E	Cow	*Bos taurus*	B7
Human	*Homo sapiens*	Hs	Sheep	*Ovis aries*	B8
Black flying fox	*Pteropus alecto*	Pa	White-tailed deer	*Odocoileus virginianus texanus*	B9
African green monkey	*Chlorocebus sabaeus*	A1	Killer whale	*Orcinus orca*	B10
Coquerel's sifaka	*Propithecus coquereli*	A2	Common bottlenose dolphin	*Tursiops truncatus*	B12
Black-capped squirrel monkey	*Saimiri boliviensis*	A3	Ferret	*Mustela putorius furo*	C1
Angola colobus	*Colobus angolensis*	A4	Cat	*Felis catus*	C2
Chimpanzee	*Pan troglodytes*	A5	Dog	*Canis lupus familiaris*	C3
Crab-eating macaque	*Macaca fascicularis*	A6	Grizzly bear	*Ursus arctos horribilis*	C4
Rhesus macaque	*Macaca mulatta*	A7	Harbor (common) seal	*Phoca vitulina*	C5
Large flying fox	*Pteropus vampyrus*	A9	California sea lion	*Zalophus californianus*	C6
Velvety free tailed bat	*Molossus molossus*	A10	Nine-banded armadillo	*Dasypus novemcinctus*	C7
Greater horseshoe bat	*Rhinolophus ferrumequinum*	A11	Chinese pangolin	*Manis pentadactyla*	C8
Pale spear-nosed bat	*Phyllostomus discolor*	A12	European rabbit	*Oryctolagus cuniculus*	C9
Big brown bat	*Eptesicus fuscus*	B1	African savannah elephant	*Loxodonta africana*	C10
Kuhl's pipistrelle	*Pipistrellus kuhlii*	B2	Cape elephant shrew	*Elephantulus edwardii*	C11
Natal long-fingered bat	*Miniopterus natalensis*	B3	Linnaeus's two-toed sloth	*Choloepus didactylus*	C12
Horse 1	*Equus caballus*	B4	Ord's kangaroo rat	*Dipodomys ordii*	D1
Pig	*Sus scrofa*	B5	Chinchilla	*Chinchilla lanigera*	D2
Dromedary camel	*Camelus dromedarius*	B6	Horse 2	*Equus caballus*	D3

Supplementary Figure 2. IFIT1 ortholog expression varied during the ortholog screen. A. Western blot from lysates of cells expressing HA-tagged IFIT1 orthologs for screen in Fig 1A demonstrating unequal IFIT1 expression patterns. Images are representative of three independent replicates. B. Key denoting which symbols correspond to HA-tagged IFIT1 ortholog. Red asterisk marks the size of the truncated or cleaved protein product in lane A3.

733

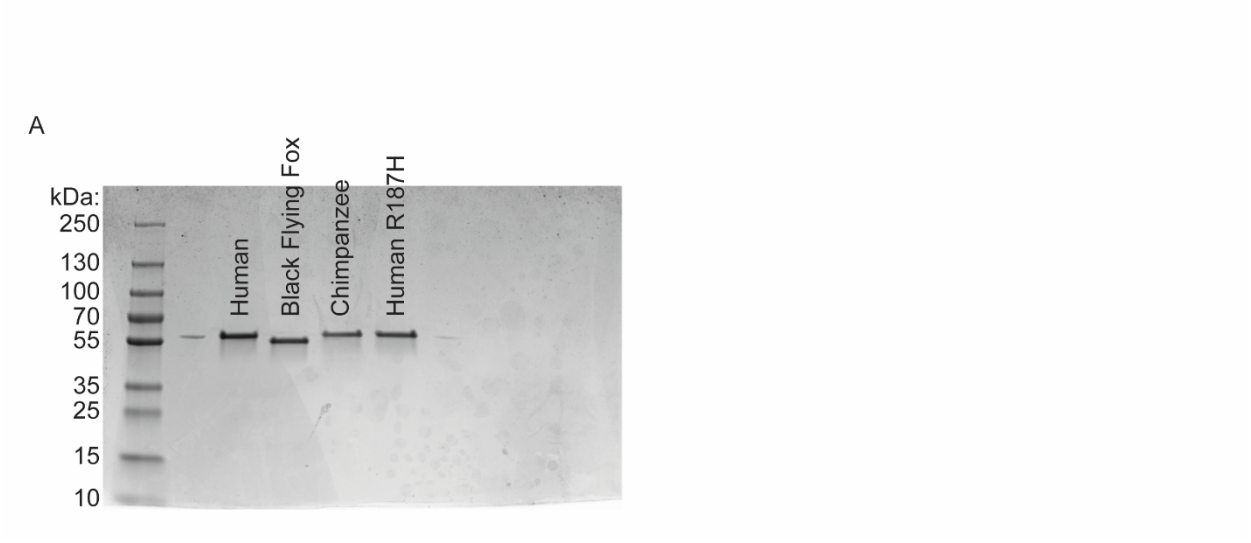

734

735

736 **Supplementary Figure 3. Gel image of recombinant IFIT1 protein.** A. Coomassie stained
737 SDS-PAGE gel of purified IFIT1 protein used for RNA EMSA.

Supplementary Table 1. Mammalian IFIT1 ortholog characteristics and antiviral activity

					Antiviral activity (% of control)					
Common name	Species	Order	Superorder	% identity to human	VEEV rep1	VEEV rep2	VSV rep1	VSV rep2	VSV rep3	NCBI sequence (CDS)
Human	Homo sapiens	Primate	Euarchontoglires	100	8.7	37.3	60.7	75.3	82.6	NM_001548.5
African green monkey	Chlorocebus sabaeus	Primate	Euarchontoglires	89.5	50.9	28.5	67.5	79.5	73.0	XM_007963500.2
Coquerel's sifaka	Propithecus coquereli	Primate	Euarchontoglires	79.1	110.1	53.1	73.7	81.6	74.9	XM_012659752.1
Black-capped squirrel monkey	Saimiri boliviensis	Primate	Euarchontoglires	88.7	281.6	79.9	94.8	88.5	78.6	XM 003922412.2
Angola colobus	Colobus angolensis	Primate	Euarchontoglires	91	26.5	9.3	69.2	74.5	66.6	XM_011947865.1
Chimpanzee	Pan troglodytes	Primate	Euarchontoglires	98.3	188.0	52.4	59.7	79.7	79.0	NM_001205347.1
Crab-eating macaque	Macaca fascicularis	Primate	Euarchontoglires	89.7	134.2	19.8	86.4	87.1	86.1	XM 015455916.1
Rhesus macaque	Macaca mulatta	Primate	Euarchontoglires	91.4	93.7	54.3	75.0	83.6	72.0	XM_015147649.2
Black flying fox	Pteropus alecto	Chiroptera	Laurasiatheria	69.1	4.9	13.9	106.2	99.2	99.8	XM_006925964.3
Large flying fox	Pteropus vampyrus	Chiroptera	Laurasiatheria	69.2	24.3	32.5	71.4	88.5	69.5	XM_011361637.2
Velvety free tailed bat	Molossus molossus	Chiroptera	Laurasiatheria	65.1	91.1	40.9	93.8	87.1	82.8	XM_036265954.1
Greater horseshoe bat	Rhinolophus ferrumequinum	Chiroptera	Laurasiatheria	69.1	299.4	115.7	87.0	79.7	79.9	XM_033131324.1
Pale spear-nosed bat	Phyllostomus discolor	Chiroptera	Laurasiatheria	65.3	224.7	103.9	82.1	87.9	97.7	XM_028512707.2
Big brown bat	Eptesicus fuscus	Chiroptera	Laurasiatheria	68.5	22.7	22.2	75.0	89.9	96.3	XM_008156938.2
Kuhl's pipistrelle	Pipistrellus kuhlii	Chiroptera	Laurasiatheria	66.4	130.4	68.5	86.7	99.7	73.2	XM_036438510.1
Natal long-fingered bat	Miniopterus natalensis	Chiroptera	Laurasiatheria	67.6	71.5	51.6	67.9	80.3	70.1	XM_016220858.1
Horse 1	Equus caballus	Perissodactyla	Laurasiatheria	68.3	306.3	124.0	79.5	83.6	78.2	XM_005602371.3
Horse 2	Equus caballus	Perissodactyla	Laurasiatheria	68.8	67.7	85.4	101.9	107.9	96.3	XM_023642993.1
Pig	Sus scrofa	Artiodactyla	Laurasiatheria	66.6	131.6	49.6	34.1	44.4	49.0	NM_001244363.1
Dromedary camel	Camelus dromedarius	Artiodactyla	Laurasiatheria	65.8	11.6	10.7	58.1	71.2	90.9	XM_010996286.2
Cow	Bos taurus	Artiodactyla	Laurasiatheria	65.9	63.9	32.4	20.7	42.5	58.3	XM_024986120.1
Sheep	Ovis aries	Artiodactyla	Laurasiatheria	64.2	2.7	7.0	65.3	79.5	57.1	XM_004020283.4
White-tailed deer	Odocoileus virginianus texanu	Artiodactyla	Laurasiatheria	68.6	3.5	9.3	29.0	57.8	45.4	XM_020894471.1
Killer whale (Orca)	Orcinus orca	Artiodactyla	Laurasiatheria	66.5	5.5	16.9	1.2	2.5	2.3	XM_012536578.2
Common bottlenose dolphin	Tursiops truncatus	Artiodactyla	Laurasiatheria	66.9	98.7	66.1	2.9	8.9	6.1	XM_019941810.2
Ferret	Mustela putorius furo	Carnivora	Laurasiatheria	67.9	26.5	54.3	74.0	75.3	90.0	XM_004780758.2
Cat	Felis catus	Carnivora	Laurasiatheria	69	70.3	72.4	84.4	71.5	96.9	XM_003993875.5
Dog	Canis lupus familiaris	Carnivora	Laurasiatheria	68.4	77.2	54.7	39.6	56.4	61.2	XM_843271.5
Grizzly bear	Ursus arctos horribilis	Carnivora	Laurasiatheria	69.2	115.8	53.5	72.7	79.2	80.3	XM 026504073.1
Harbor (common) seal	Phoca vitulina	Carnivora	Laurasiatheria	68	97.5	30.2	73.1	78.1	72.4	XM 032430411.1
California sea lion	Zalophus californianus	Carnivora	Laurasiatheria	68.8	170.9	49.2	87.3	83.8	86.1	XM 035724333.1
Chinchilla	Chinchilla lanigera	Rodentia	Euarchontoglires	63.7	163.9	83.9	89.0	81.9	85.1	XM_005385850.2
Ord's kangaroo rat	Dipodomys ordii	Rodentia	Euarchontoglires	63.7	231.0	76.0	56.2	64.1	79.5	XM_013017244.1
Nine-banded armadillo	Dasypus novemcinctus	Cingulata	Xenarthra	71.4	155.7	57.1	7.0	9.6	12.4	XM_004461422.3
Chinese pangolin	Manis pentadactyla	Pholidota	Laurasiatheria	69	4.3	5.0	80.2	70.1	68.0	XM_036928813.1
European rabbit	Oryctolagus cuniculus	Lagomorphia	Euarchontoglires	61.2	234.8	102.0	2.3	8.9	10.0	XM_008270173.2
African savannah elephant	Loxodonta africana	Proboscidea	Afrotheria	68.1	2.2	2.9	34.1	43.6	47.1	XM_023546938.1
Linnaeus's two-toed sloth	Choloepus didactylus	Pilosa	Xenarthra	72.3	34.7	48.8	25.1	44.4	47.3	XM_037804440.1
Cape elephant shrew	Elephantulus edwardii	Macroscelidea	Afrotheria	60.7	114.6	84.3	3.2	3.8	5.5	XM_006880403.1

References

1. Hyde JL, Gardner CL, Kimura T, White JP, Liu G, Trobaugh DW, et al. A viral RNA structural element alters host recognition of nonself RNA. Science. 2014;343(6172):783-7.
2. Pichlmair A, Lassnig C, Eberle CA, Gorna MW, Baumann CL, Burkard TR, et al. IFIT1 is an antiviral protein that recognizes 5'-triphosphate RNA. Nat Immunol. 2011;12(7):624-30.
3. Abbas YM, Laudenbach BT, Martinez-Montero S, Cencic R, Habjan M, Pichlmair A, et al. Structure of human IFIT1 with capped RNA reveals adaptable mRNA binding and mechanisms for sensing N1 and N2 ribose 2'-O methylations. Proc Natl Acad Sci U S A. 2017;114(11):E2106-E15.
4. Diamond MS, Farzan M. The broad-spectrum antiviral functions of IFIT and IFITM proteins. Nat Rev Immunol. 2013;13(1):46-57.
5. Hyde JL, Diamond MS. Innate immune restriction and antagonism of viral RNA lacking 2-O methylation. Virology. 2015;479-480:66-74.
6. Daugherty MD, Malik HS. Rules of engagement: molecular insights from host-virus arms races. Annu Rev Genet. 2012;46:677-700.
7. Duggal NK, Emerman M. Evolutionary conflicts between viruses and restriction factors shape immunity. Nat Rev Immunol. 2012;12(10):687-95.
8. Sironi M, Cagliani R, Forni D, Clerici M. Evolutionary insights into host-pathogen interactions from mammalian sequence data. Nat Rev Genet. 2015;16(4):224-36.
9. Mitchell PS, Patzina C, Emerman M, Haller O, Malik HS, Kochs G. Evolution-guided identification of antiviral specificity determinants in the broadly acting interferon-induced innate immunity factor MxA. Cell Host Microbe. 2012;12(4):598-604.
10. Sawyer SL, Wu LI, Emerman M, Malik HS. Positive selection of primate TRIM5alpha identifies a critical species-specific retroviral restriction domain. Proc Natl Acad Sci U S A. 2005;102(8):2832-7.
11. Daugherty MD, Schaller AM, Geballe AP, Malik HS. Evolution-guided functional analyses reveal diverse antiviral specificities encoded by IFIT1 genes in mammals. Elife. 2016;5.
12. Cruz-Rivera PCDL, Eitson JL, Schoggins JW. IRF7 from the black flying fox induces a STAT1-independent ISG response in unstimulated cell lines that protects against diverse RNA viruses. bioRxiv. 2024:2024.05.02.592239.
13. Yang Z. PAML 4: phylogenetic analysis by maximum likelihood. Mol Biol Evol. 2007;24(8):1586-91.
14. Murrell B, Moola S, Mabona A, Weighill T, Sheward D, Kosakovsky Pond SL, et al. FUBAR: a fast, unconstrained bayesian approximation for inferring selection. Mol Biol Evol. 2013;30(5):1196-205.
15. Murrell B, Wertheim JO, Moola S, Weighill T, Scheffler K, Kosakovsky Pond SL. Detecting individual sites subject to episodic diversifying selection. PLoS Genet. 2012;8(7):e1002764.
16. Kosakovsky Pond SL, Posada D, Gravenor MB, Woelk CH, Frost SD. Automated phylogenetic detection of recombination using a genetic algorithm. Mol Biol Evol. 2006;23(10):1891-901.
17. Martin DP, Murrell B, Golden M, Khoosal A, Muhire B. RDP4: Detection and analysis of recombination patterns in virus genomes. Virus Evol. 2015;1(1):vev003.
18. Reynaud JM, Kim DY, Atasheva S, Rasalouskaya A, White JP, Diamond MS, et al. IFIT1 Differentially Interferes with Translation and Replication of Alphavirus Genomes and Promotes Induction of Type I Interferon. PLoS Pathog. 2015;11(4):e1004863.
19. Young DF, Andrejeva J, Li X, Inesta-Vaquera F, Dong C, Cowling VH, et al. Human IFIT1 Inhibits mRNA Translation of Rubulaviruses but Not Other Members of the Paramyxoviridae Family. J Virol. 2016;90(20):9446-56.
20. Rabbani MA, Ribaudo M, Guo JT, Barik S. Identification of Interferon-Stimulated Gene Proteins That Inhibit Human Parainfluenza Virus Type 3. J Virol. 2016;90(24):11145-56.

21. Hankinson J, Young D, Wignall-Fleming EB, Lukoszek R, Cowling VH, Randall R, et al. The Cap-proximal secondary structures of the 5'UTRs of parainfluenza virus 5 mRNAs specify differential sensitivity to type I interferon and IFIT1. J Gen Virol. 2025;106(3).
22. Andrejeva J, Norsted H, Habjan M, Thiel V, Goodbourn S, Randall RE. ISG56/IFIT1 is primarily responsible for interferon-induced changes to patterns of parainfluenza virus type 5 transcription and protein synthesis. J Gen Virol. 2013;94(Pt 1):59-68.
23. Halpin K, Young PL, Field HE, Mackenzie JS. Isolation of Hendra virus from pteropid bats: a natural reservoir of Hendra virus. J Gen Virol. 2000;81(Pt 8):1927-32.
24. Marsh GA, de Jong C, Barr JA, Tachedjian M, Smith C, Middleton D, et al. Cedar virus: a novel Henipavirus isolated from Australian bats. PLoS Pathog. 2012;8(8):e1002836.
25. Barr JA, Smith C, Marsh GA, Field H, Wang LF. Evidence of bat origin for Menangle virus, a zoonotic paramyxovirus first isolated from diseased pigs. J Gen Virol. 2012;93(Pt 12):2590-4.
26. Boys IN, Xu E, Mar KB, De La Cruz-Rivera PC, Eitson JL, Moon B, et al. RTP4 Is a Potent IFN-Inducible Anti-flavivirus Effector Engaged in a Host-Virus Arms Race in Bats and Other Mammals. Cell Host Microbe. 2020;28(5):712-23 e9.
27. Hayward JA, Tachedjian M, Cui J, Cheng AZ, Johnson A, Baker ML, et al. Differential Evolution of Antiretroviral Restriction Factors in Pteropid Bats as Revealed by APOBEC3 Gene Complexity. Mol Biol Evol. 2018;35(7):1626-37.
28. Hayward JA, Tachedjian M, Johnson A, Irving AT, Gordon TB, Cui J, et al. Unique Evolution of Antiviral Tetherin in Bats. J Virol. 2022;96(20):e0115222.
29. Morrison JH, Miller C, Bankers L, Crameri G, Wang LF, Poeschla EM. A Potent Postentry Restriction to Primate Lentiviruses in a Yinpterochiropteran Bat. mBio. 2020;11(5).
30. Ohkura S, Horie M, Shimizu M, Nakagawa S, Osanai H, Miyagawa Y, et al. Characterization of Megabat-Favored, CA-Dependent Susceptibility to Retrovirus Infection. J Virol. 2023;97(3):e0180322.
31. Zhang Q, Zeng LP, Zhou P, Irving AT, Li S, Shi ZL, et al. IFNAR2-dependent gene expression profile induced by IFN-alpha in Pteropus alecto bat cells and impact of IFNAR2 knockout on virus infection. PLoS One. 2017;12(8):e0182866.
32. Chan SH, Mole CN, Nye D, Mitchell L, Dai N, Buss J, et al. Biochemical characterization of mRNA capping enzyme from Faustovirus. RNA. 2023;29(11):1803-17.
33. Fensterl V, Sen GC. Interferon-induced Ifit proteins: their role in viral pathogenesis. J Virol. 2015;89(5):2462-8.
34. Tenthorey JL, Young C, Sodeinde A, Emerman M, Malik HS. Mutational resilience of antiviral restriction favors primate TRIM5alpha in host-virus evolutionary arms races. Elife. 2020;9.
35. Mears HV, Sweeney TR. Better together: the role of IFIT protein-protein interactions in the antiviral response. J Gen Virol. 2018;99(11):1463-77.
36. Geng J, Chrabaszczewska M, Kurpiejewski K, Stankiewicz-Drogon A, Jankowska-Anyszka M, Darzynkiewicz E, et al. Cap-related modifications of RNA regulate binding to IFIT proteins. RNA. 2024;30(10):1292-305.
37. Johnson B, VanBlargan LA, Xu W, White JP, Shan C, Shi PY, et al. Human IFIT3 Modulates IFIT1 RNA Binding Specificity and Protein Stability. Immunity. 2018;48(3):487-99 e5.
38. Xie S, Fang Y, Liao Z, Cui L, Niu K, Ren S, et al. A poxvirus ankyrin protein LSDV012 inhibits IFIT1 in a host-species-specific manner by compromising its RNA binding ability. PLoS Pathog. 2025;21(3):e1012994.
39. Atasheva S, Krendelchtchikova V, Liopo A, Frolova E, Frolov I. Interplay of acute and persistent infections caused by Venezuelan equine encephalitis virus encoding mutated capsid protein. J Virol. 2010;84(19):10004-15.
40. Simmons JD, Wollish AC, Heise MT. A determinant of Sindbis virus neurovirulence enables efficient disruption of Jak/STAT signaling. J Virol. 2010;84(21):11429-39.

41. Kane M, Zang TM, Rihn SJ, Zhang F, Kueck T, Alim M, et al. Identification of Interferon-Stimulated Genes with Antiretroviral Activity. Cell Host Microbe. 2016;20(3):392-405.
42. Kumar S, Stecher G, Li M, Knyaz C, Tamura K. MEGA X: Molecular Evolutionary Genetics Analysis across Computing Platforms. Mol Biol Evol. 2018;35(6):1547-9.
43. Castresana J. Selection of conserved blocks from multiple alignments for their use in phylogenetic analysis. Mol Biol Evol. 2000;17(4):540-52.
44. Glez-Pena D, Gomez-Blanco D, Reboiro-Jato M, Fdez-Riverola F, Posada D. ALTER: program-oriented conversion of DNA and protein alignments. Nucleic Acids Res. 2010;38(Web Server issue):W14-8.
45. Murrell B, Weaver S, Smith MD, Wertheim JO, Murrell S, Aylward A, et al. Gene-wide identification of episodic selection. Mol Biol Evol. 2015;32(5):1365-71.
46. Kosakovsky Pond SL, Poon AFY, Velazquez R, Weaver S, Hepler NL, Murrell B, et al. HyPhy 2.5-A Customizable Platform for Evolutionary Hypothesis Testing Using Phylogenies. Mol Biol Evol. 2020;37(1):295-9.
47. Weaver S, Shank SD, Spielman SJ, Li M, Muse SV, Kosakovsky Pond SL. Datamonkey 2.0: A Modern Web Application for Characterizing Selective and Other Evolutionary Processes. Mol Biol Evol. 2018;35(3):773-7.
48. Kumar S, Stecher G, Suleski M, Hedges SB. TimeTree: A Resource for Timelines, Timetrees, and Divergence Times. Mol Biol Evol. 2017;34(7):1812-9.
49. Sievers F, Wilm A, Dineen D, Gibson TJ, Karplus K, Li W, et al. Fast, scalable generation of high-quality protein multiple sequence alignments using Clustal Omega. Mol Syst Biol. 2011;7:539.
50. Meng EC, Goddard TD, Pettersen EF, Couch GS, Pearson ZJ, Morris JH, et al. UCSF ChimeraX: Tools for structure building and analysis. Protein Sci. 2023;32(11):e4792.